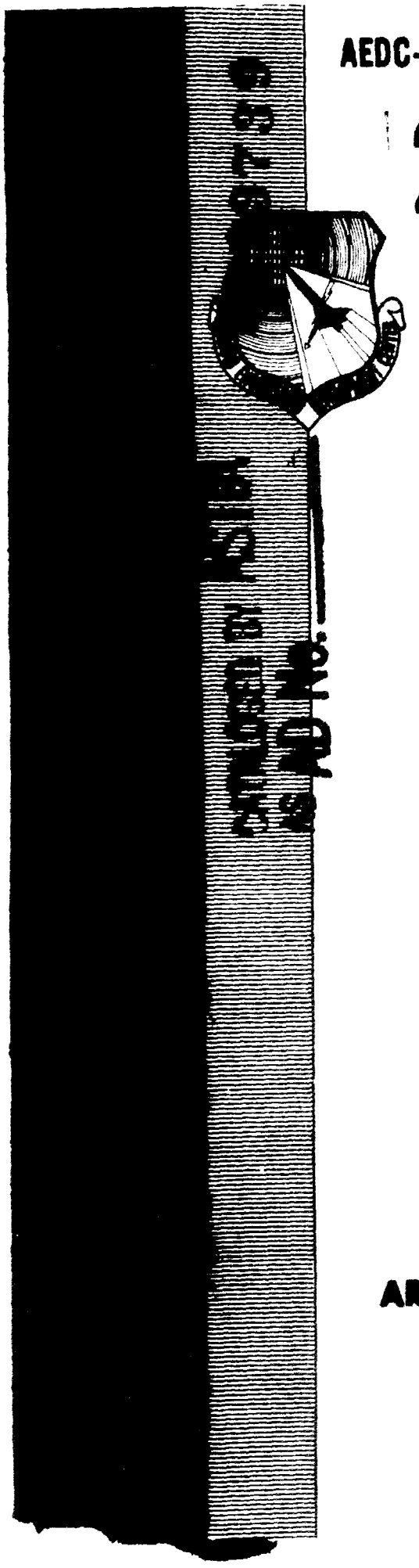

RESEARCH STUDY OF CRYOPUMPING WITH A RADIATION SHIELDED CONDENSER

By

Raymond W. Moore, Jr.
Arthur D. Little, Inc.

TECHNICAL DOCUMENTARY REPORT NO. AEDC-TDR-62-57

March 1962

AFSC Program Area 850E, Project 7778, Task 777801

(Prepared under Contract No. AF 40(600)-899 by
Arthur D. Little, Inc., Cambridge, Massachusetts)

ARNOLD ENGINEERING DEVELOPMENT CENTER
AIR FORCE SYSTEMS COMMAND
UNITED STATES AIR FORCE

RESEARCH STUDY OF CRYOPUMPING WITH A RADIATION SHIELDED CONDENSER

By

Raymond W. Moore, Jr.

Arthur D. Little, Inc.

(The reproducible copy supplied by Arthur D. Little, Inc. was used in the reproduction of this report.)

March 1962

ABSTRACT

The purpose of this study was to develop information for the empirical design of a cryopumping array. Experiments with a chevron-shielded condenser have been carried out and, where possible, the results correlated with analysis. An array constructed from aluminum panels proved to be very serviceable. The array capture probability for nitrogen was about 0.2 and was essentially constant over the range of pressures from 10^{-8} to 5×10^{-6} torr; above 5×10^{-6} torr the capture probability increased with pressure. CO_2 was cryopumped on the chevron shields. Hence, the capture probability was high, varying from 0.7 to 0.94 in the pressure range from 5×10^{-7} to 7×10^{-5} torr.

The greatest transmission of radiation through the chevrons to the condenser occurred with a CO_2 deposit on the chevrons and a nitrogen deposit on the condenser, and with infrared radiation incident on the inlet to the array. Even under these conditions less than 2 percent of the incident irradiation was transmitted to the condenser.

As a result of our study, we conclude that cryopumping by means of a condenser at 20 K, radiation shielded by surfaces cooled to 77 to 100 K, can provide effective means for removal of nitrogen and all less volatile gases from a vacuum space in the ultra-high vacuum range.

TABLE OF CONTENTS

TABLE OF CONTENTS (Cont'd.)

LIST OF TABLES

LIST OF FIGURES

I. SUMMARY

A. PURPOSE AND SCOPE

The purpose of the experimentation and analysis comprising this study was to develop information for the empirical design of a cryopumping array. It was originally intended that several configurations of cryopumping arrays would be investigated. However, the effort required to get useful quantitative results by experimentation was considerably greater than anticipated. As a result, only one cryopumping array configuration, a flat tubed-sheet condenser shielded by chevrons, was investigated. The results of our work on the chevron array are presented in this report. Included is information on the cryopumping of nitrogen and carbon dioxide, the removal of non-condensables (hydrogen), the heat loads on the cryogenic surfaces with both infrared and solar irradiation, and the composition of residual gases in the chamber during cryopumping. A description of the apparatus and its operation is also presented.

B. CONCLUSIONS

Cryopumping by means of a 20 K condenser, radiation shielded with surfaces cooled to 77 K to 100 K, can provide effective means for the removal of nitrogen and all less volatile gases from a vacuum space in the ultra-high vacuum region. The capture probability for nitrogen of the chevron-shielded condenser used in our experiments was approximately 0.2 and was relatively independent of pressure over the range from 10^{-8} to 5×10^{-6} torr. This value of capture probability corresponds to a pumping speed per unit of inlet area of 81 cu. ft./sec - ft^2. Above 5×10^{-6} torr, the capture probability increased with pressure.

In our apparatus the chevron radiation shields were cooled to about 77 K. Consequently, CO_2 was cryopumped by the chevrons at pressures higher than about 1.5×10^{-8} torr. The capture probability for CO_2 was a function of the amount of deposit on the chevrons; the high capture probability that one would associate with cryopumping by the exposed chevrons, was not realized until a certain amount of condensate had accumulated on the surfaces. Once the condensate had accumulated, capture probabilities ranging from 0.7 to 0.94 were observed in the pressure range of 4.6×10^{-7} to 6.8×10^{-5} torr. With CO_2 deposited on the chevrons, the ultimate pressure in the chamber was limited to about 1.5×10^{-8} torr.

Non-condensables were removed by a conventional diffusion pumping system consisting of a ten-inch and a two-inch diffusion pump in series. The pumping speed of the diffusion pumping system was considerably limited by the arrangement of cryogenic panels upstream, a condition unique to our particular experimental set-up. The pumping speed for hydrogen, approximately 30 cu ft./sec., was essentially constant over the pressure range of 10^{-8} to 10^{-5} torr.

Observations of the pressure in the chamber as the condenser temperature was varied from 20 to 13 K suggested that small amounts of hydrogen are adsorbed on the condenser.

Considerable difficulty was encountered in measuring heat loads on the cryogenic surfaces, particularly in measuring the heat load on the condenser. The difficulties were associated with the low level of the load, which was about 1.5 watts. Nevertheless, it is clear that the chevron radiation shields provided effective shielding even when there were condensed deposits on both the chevrons and the condenser. The greatest transmission of radiation through the chevrons to the condenser occurred with a CO_2 deposit on the chevrons and a nitrogen deposit on the condenser and with infrared radiation incident on the inlet to the array. Even under these conditions less than 2 percent of the incident irradiation was transmitted to the condenser.

The residual gas in the chamber was analyzed by an Omegatron mass spectrometer during cryopumping, and with a chamber pressure of 8×10^{-9} torr upstream of the chevrons and 5×10^{-9} torr adjacent to the condenser. The partial pressures of hydrogen and helium were insignificant in comparison to the partial pressures of gases represented by mass numbers 12 through 14, and 25 through 32 in the Omegatron analysis. We attribute the presence of these mass numbers in the test to outgassing of air and hydrocarbons from the inside of the Omegatron.

The aluminum panels from which the array was constructed have proven satisfactory and serviceable. After initial leak detection and repair, the vacuum integrity of both the cryopanels and the stainless steel chamber was maintained over a period of seven months. During this time, approximately 35 tests were carried out in which the panels were cooled down and held at operating temperatures for periods averaging about six hours; no significant leakage developed in any of the welded joints in either the cryopanels or the tank.

In our experiments, we used hot cathode ion gages for pressure measurement below 10^{-5} torr. It became clear that even the use of the best operating techniques currently known did not insure accurate and reliable pressure measurement below about 10^{-4} torr; hence, the determinations of pumping speed, ultimate pressure and other gas flow performance characteristics were compromised. As a minimum requirement for making quantitative measurements, ultra-high vacuum gages must be frequently compared to a suitable standard, such as the McLeod gage, in a way which minimizes the errors involved in extrapolating gage factors to the ultra-high vacuum range.

C. RECOMMENDATIONS

As a result of our studies we recommend that:

1. Cryopumping with a 20 K condenser radiation shielded by liquid-nitrogen cooled surfaces, be considered as a practical and effective way of achieving very high pumping speeds for nitrogen and less volatile gases at pressures down to at least 10^{-6} torr.

2. The chevron-shielded condenser be considered for applications where minimum transmission of energy to the 20 K condenser, per unit of pumping speed is desired.

3. Further measurements of heat loads on the cryogenic surfaces be carried out, preferably on a larger scale and under operating conditions like those which will be encountered in practice.

4. Liquid-nitrogen cooled radiation shields be operated at a temperature of about 100 K to prevent the cryopumping of CO_2 on the shields in applications where it will be pregent in substantial amounts and where chamber pressures below about 1.5×10^{-6} torr are required.

5. Aluminum panel construction of the type used in this investigation be considered as a practical way of fabricating cryopanels.

II. INTRODUCTION

Previous studies conducted by Arthur D. Little, Inc., (ADL) and others,[1][2]* strongly suggest that the most practical and economical way to provide high pumping speeds for most gases is by the use of cryopumping. This is particularly true for the space simulation chamber application where both the thermal and vacuum simulation can be accomplished by a suitably designed arrangement of cryogenically-cooled panels (cryopanels). Prior to this investigation, very little work of an experimental nature had been done on cryopumping, and to a large extent the present investigation has been an attempt to validate experimentally the conclusions reached in analytical studies with regard to pumping speeds and heat load on the 20 K condenser.

ADL's interest in cryopumping led to the establishment of a company-sponsored research project to investigate the performance of a chevron-shielded condenser in February 1960. Under this project a high-vacuum chamber was constructed and tested, and the cryo-array, shown in Figure 1, was fabricated by welding aluminum tubes to flat aluminum surfaces in the desired geometry. The welded-type construction proved to be unsatisfactory. Considerable difficulty was encountered during fabrication with thermal warpage and burn-throughs. In a number of places a gas pocket was formed by the tube, the weld and the sheet; any leak through the weld would permit outgassing into the vacuum space. Such leakage could not be located by known detection techniques. Moreover, the welding of coolant tubes to the sheets proved to be time-consuming and very costly and in our opinion would only be suitable for small test apparatus.

Air Force sponsorship of experimental work on cryopumping, under the present contract, began at the end of July 1960. Shortly after the beginning of work under Air Force sponsorship we concluded that the leakage and outgassing problems associated with the welded array construction appeared insurmountable and decided to replace the array that had been constructed for the ADL Research Project. At that time we turned to a construction which made use of "tubed sheet", a product of the Reynolds Metals Company. A second array was fabricated and it proved to be highly satisfactory after initial leak testing and repair. Not only were the leakage and outgassing problems associated with the welded-type construction eliminated, but also the design, fabrication and test experience gained with these panels is more directly applicable to large chambers. The

*Superscripts in parentheses designate references which are listed at the end of the report

vacuum chamber which had been constructed under the ADL Research Project, was, readily adaptable to the Air Force program and it was used throughout the tests.

Experimentation with the apparatus began in December 1960 and the tests reported herein were conducted in the period from January 1961 through August 1961. Air Force funding for the experimental work was depleted by July 1961. At that time, good information had not yet been obtained on the cryopumping of CO_2, the heat loads on the cryopanels, and the composition of the residual gases in the chamber while cryopumping. Because these items were of considerable interest to both Arnold Engineering Development Center and ADL, ADL established a second research project to complete them. Useful results on the cryopumping of CO_2, on the cryogenic heat loads and on the composition of the residual gases in the chamber, were obtained under this research project. They are included in this report.

National Research Corporation (NRC), under subcontract, assisted ADL in vacuum instrumentation, ion gage calibrations and pumping speed determinations. A summary of their work, as prepared by NRC, is included in Appendix D. Their report is complete in itself, including a Table of Contents and References.

III. APPARATUS AND MEASUREMENTS

A. GENERAL

The set-up of equipment, including the chamber, refrigeration sources, and instrumentation, is shown in Figure 2. The various components are identified in the tabulation on the figure. A flow sheet for the system is presented in Figure 3. The functions of the various components and instruments are indicated in the sections which follow.

B. CHAMBER AND CRYOPANELS

A cross section through the cryopump vacuum test chamber is shown in Figure 4. Input gases were introduced at the right and flowed through screens to the array inlet. The screens distributed the gas so as to produce uniform flow into the array. Condensables were deposited as solids either on the chevrons or on the 20 K condenser. Non-condensable gases continued through the array, and through a 10-inch 90° elbow to the inlet of a diffusion pump system (described in Section III-E). The surfaces surrounding the 20 K condenser provided radiation shielding. They were cooled with liquid nitrogen to 77 K. The chevrons permit gas flow to the condenser, but minimize the transmission of radiant heat energy to the condenser from the front. The back shields permit non-condensables to flow to the diffusion pump but, along with the outer shields, prevent radiation from the warm tank walls from striking the condenser. The surfaces were made either highly absorptive (black) or highly reflective, as indicated in Figure 4, to minimize radiant heat transmission to the condenser.

In some tests, which will be described, it was desirable to irradiate the inlet to the array (that is, the right edge of the chevrons) with solar and infrared energy. For this purpose the flow distributing screens were removed. Solar irradiation was admitted through the sapphire window at the right, while infrared irradiation was supplied from a bulb mounted inside the tank. (These radiation sources are described in Sections III-F and III-G below).

Photographs of the cryo-array and the vacuum chamber are shown in Figures 5 and 6. In Figure 5 the panels visible are, from right to left, the chevrons, the 20 K condenser (with vertical slots), and the two back shields. In Figure 6, the outer shields are visible. The chamber, three feet in diameter and four feet long, was constructed of Type 321 stainless steel; heli-arc welding was used throughout. The inner surface was polished, as can be seen in Figure 6.

The cryo-array has been completely described in a Progress Report[3] It was fabricated as part of this project by ADL using Reynolds Metals Co.'s "tubed-sheet". The panels and piping were all aluminum up to points near where the warm wall of the tank was penetrated. There, stainless steel-to-aluminum transition joints were inserted so that only stainless steel lines penetrated the stainless steel tank. Heli-arc welding was used throughout. Initial leak testing of the array revealed a number of leaks in welded joints. However, only one leak, a "pinhole" in a header tube, was found in a panel. Conventional helium mass spectrometer techniques were used to detect leaks; repair was accomplished by welding over. A final leak test with all the cryopanels cooled to liquid-nitrogen temperature revealed that the total equivalent inleakage of air to the vacuum space from the cryopanels and from outside the tank was no greater than about 5×10^{-7} scc/sec. At a pressure of 10^{-8} torr this mass flow corresponds to a volume flow of about 38 liters/sec. (1.35 cu.ft./sec.), which is small compared to the pumping speed of the diffusion pumping system alone. Thus, at a pressure of 10^{-8} torr, this flow has no significant effect on tests.

To make the chevrons and portions of other surfaces highly absorptive for both solar and infrared energy, we had them grit-blasted and then subjected to a heavy black anodize. The reflective surfaces on the shields and condenser were chemically polished in the "as received" condition. Because of the nature of the manufacturing process, the "as received" finish was fairly smooth and the surface which resulted from chemical polishing was highly reflective. The radiation properties of these two types of surfaces, have been described in some detail in a Progress Report[4]

C. CRYOGENIC CIRCUITS AND INSTRUMENTATION

Operation of the cryo-array requires refrigeration at two levels: one at 77 K and the other between 15 and 20 K. Refrigeration at the higher temperature level was provided by the vaporization of liquid nitrogen supplied from the storage tank shown in Figure 2. The liquid nitrogen supplied cooling for the chevrons, back shields, outer shields and diffusion pump baffle, and pre-cooling for the 20 K refrigerator. To insure that liquid entering the chevrons was saturated at a known pressure, a gas-liquid separator was included in the feed line, as indicated in Figure 3. The two-phase mixture of gas and liquid from the transfer line flowed into the vacuum-jacketed separator pot. The pot was kept about half full of liquid; saturated liquid was drawn off through the bottom while the flash gas from the transfer process was exhausted from the top. By eliminating vapor from the feed to the chevrons, we insured that the vapor exhaust from the chevrons was attributable to the heat load on them. The vapor exhaust flow passed through a warm-up tube and was metered with an orifice.

Refrigeration at the 20 K level was supplied by an ADL-Collins Helium Cryostat, Refrigerator Model. This unit circulated cold helium gas to the

condenser in the vacuum test chamber. The gas flowed from the cryostat through an inlet temperature control heater, into the condenser panel and back to the cryostat through a calorimetric mass flowmeter, as shown in Figure 3. Throttling valves in the outlet and return lines and a by-pass valve, all in the cryostat, were used for regulating the flow to the condenser.

The inlet and outlet temperatures of the condenser (T_1 and T_2, Figure 3) and of the calorimetric flowmeter (T_3 and T_4) were measured with liquid-hydrogen vapor-pressure thermometers. The thermometers each consisted of a sensing bulb connected through a 0.093 in. ID x 5 ft. long capillary to a warm (room temperature) reservoir to which a 0-215 psia Helicoid pressure gage was connected. Significant features were:

Sensing bulb internal volume - 0.10 cu. in.

Total warm volume - 3.60 cu. in.

Capillary - 0.41

Reservoir - 2.37

Gage - 0.82

Charge pressure - 150 psia

The sensing bulbs were placed directly inside the helium lines so that they were in intimate contact with the flowing gas. The thermometers provided accurate measurements of temperature (about $\pm$ 0.1 K) over the range of 15 to 30 K.

In the calorimetric flowmeter the flowing helium gas absorbed heat at a measured input rate from an electrical heater. The temperature rise of the gas, as indicated by T_3 and T_4, combined with the heat input rate and the specific heat of helium (a known constant in the range of interest) determined the mass flow rate.

Temperatures at eight different points on the cryopanels were monitored by copper-constantan thermocouples. Each pair of thermocouple wires were contained in a 1/16-inch OD stainless steel sheath packed with powdered ceramic insulation (Thermo-electric Company's "Ceramo"). Each sheath was closed off and grounded to the measuring junction at the end. The sheaths for all the couples were welded into a stainless steel plug, which was in turn welded into the stainless steel tank. Thus, only small diameter stainless steel tubes were exposed to the vacuum. Each thermocouple had a separate reference junction which was placed in a LN_2 bath during operation. Outputs were fed into a recorder.

D. INSTRUMENTATION FOR VACUUM AND PUMPING SPEED MEASUREMENTS

1. Pressure (Vacuum) Gages

Six conventional hot-cathode ion gages, as listed below, were used for measurements below 10^{-3} torr:

Gage No.	Type	Location
P1	NRC 551, Nottingham	45° from top of tank, 4 ins. upstream of array inlet
P2	Veeco RG-75, Bayard Alpert	Teed with an Omegatron gage from tubulation sampling gas adjacent to the 20 K condenser
P3 and P4	NRC 518, Standard	Gas input plenum chambers
P5	Veeco RG-75, Bayard-Alpert	Chamber head downstream of array, near inlet to diffusion pump system
P6	Veeco RG-75, Bayard-Alpert	45° from top of tank, opposite P1

These gage locations are indicated schematically in Figures 3 and 4. Midway through the experiments a nude ion gage (Vactronic Type NIG) was installed, adjacent to P1 and in the same axial plane. A Pirani gage, at the bottom of the tank and in the same axial plane as P1 and P6, was used for measuring chamber pressures above 10^{-3} torr. All of these gages were calibrated against a McLeod gage. The calibration procedure has been fully described in Progress Reports[5]. A summary discussion of their calibration and use is presented in Appendix D. Gages P1 and P6 were used for indicating the pressure (or density) upstream of the array in pumping speed determinations.

2. Mass Flow Metering and Control

The mass flow rate inputs to the chamber, which are required for pumping speed determinations, were measured in three ways. At chamber pressures below about 10^{-6} torr, the mass flow rates were extremely small; metering with a known conductance operating in the free molecular flow regime proved to be the most practical approach. We made use of the known conductances of thin plate orifices with diameters substantially smaller than the mean-free path. A steady flow of gas was introduced to one of two plenum chambers attached to the main vacuum chamber (Figure 3) and thence flowed into the chamber through a thin plate orifice of either 1/2-inch or 3/4-inch diameter. The orifices were sized so that the downstream pressure (i.e., the pressure in the chamber) was negligibly small compared to the upstream pressure. The plenum chamber was fitted with baffles and the gas was injected in such a way that the pressure throughout the plenum was uniform. Thus, the equation for free molecular effusion through an orifice into a perfect vacuum (used in a subsequent discussion of pumping speed experiments, Section IV-B) could be applied with good accuracy. With that equation, the upstream gas pressure and temperature determine the mass flow rate. The pressure in the plenum was measured with an ion gage (P3 or P4); the temperature was assumed to be 530 R.

At chamber pressures between about 5×10^{-6} and 5×10^{-4} torr we were able to use a displacement oil manometer. A calibrated instrument was provided by MRC. The device was used to admit a known quantity of gas into the chamber through one of the gas input plenums, at a uniform rate determined by the pumping speed. Measurement of the time required for the gas to be admitted with a stop watch enabled us to determine the mass flow rate. Measurements with this device and its accuracy are further discussed in Appendix D.

At chamber pressures above about 10^{-4} torr the mass flow rate was large enough to be measured with Fischer and Porter Co. Tri-flat Flowrater tubes. Considerable difficulty was encountered with the repeatability of measurements with a 1/16-inch tube and its use was eventually discontinued. Good results were obtained with a 1/8-inch tube. The manufacturer claims an accuracy of $\pm$ 2 percent of full-scale indication.

3. Omegatron Unit

An Omegatron Mass Spectrometer unit was used to analyze the gas composition in the chamber, at a point adjacent to condenser. Although this type of instrument has become increasingly important for ultra-high vacuum work, we found no commercially available units that were "ready to use". Therefore a unit was assembled, checked out and installed under this contract. A block diagram of the unit, in which various components are identified, is shown in Figure 7. The Omegatron tube and the permanent magnet (made by Leybold) were supplied by MRC.

They also designed, built, and furnished the power supply for the tube. The oscillator, amplifier and strip chart recorder were standard units and were available at ADL. Rack mounting and electrical hook-up of the components and check-out of the unit with the tube on a separate vacuum system was carried out by ADL personnel.

The Omegatron tube and an ion gage (P2) were connected to the cryo-pumping chamber on a common tubulation. A stainless steel tube was inserted into the tubulation, inside the chamber, as shown in Figure 4, so that the Omegatron samples gas from a point inside the LN_2 radiation shields and adjacent to the 20 K condenser.

A heating tape was used to bake-out the glass tube at 400-500 F; the metal elements were outgassed at higher (dull red) temperatures with an RF induction heating coil.

E. DIFFUSION PUMP SYSTEM

The diffusion pumping system in order of proceeding downstream, consisted of a 10-inch NRC optical baffle cold trap (LN_2 cooled), an NRC H-10-SP diffusion pump, an NRC 3-inch gate valve, an NRC H-2-SP diffusion pump and a 5 CFM forepump. Placement of the 3-inch gate valve downstream of the 10-inch pump avoided its exposure to the ultra-high vacuum in the chamber. The valve enabled us to isolate the chamber from the pumping system. The 10-inch pump could not be operated with the valve shut but the 2-inch pump could be kept running.

F. SOLAR SOURCE

A solar source unit, constructed as part of the project, was used to irradiate the array with simulated solar energy. It has been fully described in Progress Reports[6]. The source was a 1000-watt Hanovia Xenon-Mercury bulb. A schematic diagram of the unit showing the optical arrangement for irradiating the array is presented in Figure 8. Figure 9 is a photograph showing the unit in operation.

The output from the solar source arriving at the array was considerably less than anticipated. The heat load tests which will be described (Section VII) revealed that about 50 to 60 watts were delivered to the use point. Thus, the over-all efficiency of the source and transmission system was only about 5-6 percent.

G. INFRARED SOURCE

A GE 250-watt heat lamp was used as an infrared source. It was mounted inside the chamber so that it irradiated the chevrons. Figure 10 shows the lamp arrangement, as viewed looking upstream from the array (the array has been removed; the lamp is in the upper center). The manufacturer's literature shows that its output has a maximum intensity at a wavelength of about 1.3 microns. The lamp produced some 50-60 watts of IR irradiation on the chevrons.

H. BAKE-OUT OVEN

It was initially thought that bake-out of the chamber would be required to achieve the low ultimate pressure required for making good pumping speed measurements at 10^{-8} torr. The oven shown in Figure 11 was constructed for such bake-out. It was designed so that it could be rolled into place around the chamber. Electrical heaters mounted along its wall and a circulation fan can be seen in the photo. The head of the vacuum tank was not intended to be baked out, due to the numerous penetrations in it. The doors to the oven fit around the tank at a position adjacent to the main flange. During bake-out the "O" ring seal for the main flange was cooled by water flowing through jackets adjacent to the flange.

We found in early runs that a sufficiently low ultimate pressure could be reached without bake-out, so that except for a few tests early in the program, bake-out was not used.

IV. CRYOPUMPING OF NITROGEN

A. GENERAL

The vapor pressure of N_2 at 20 K is about 10^{-11} torr[7]. At any higher pressure, the gas will be cryopumped on the 20 K condenser. The rate at which nitrogen will be pumped in the free molecule flow regime is most effectively described by the "capture probability" of the array; that is, the fraction of molecules incident on the array which pass through the chevrons and are condensed on the 20 K surface without rebounding back into the space upstream of the chevrons. As we will show, this quantity is directly related to the more familiar "pumping speed".

Our approach has been to, first, experimentally determine the pumping speed, and then, using the results of analysis, to deduce the array capture probability and the condenser sticking coefficient. We define the pumping speed, in terms of the upstream gas density indicated by gage P1 or P6 (Figure 4) as follows:

$$1) \quad Q_o = \frac{W}{m\, n_p}$$

Where Q_p is the pumping speed, W is the mass flow rate, m is the mass of a molecule and n_p is the molecular density of gas upstream of the array indicated by the probe. Assuming the gas inside the probe is an equilibrium gas at the probe temperature, T_p, and that it has a pressure, P_p, we find that:

$$2) \quad n_p = \frac{P_p}{k\, T_p}$$

where k = Boltzmann's constant so that

$$3) \quad Q_p = \frac{W\, k\, T_p}{m\, P_p}$$

B. PUMPING SPEED

Experimental determination of the pumping speed defined by Equation (3) necessitated measurement of P_p, (with gage P1 or P6) and W as described in Section III-D; T_p was taken to be 530 R. When the orifice technique was used for determining W, the equation for mass flow was

$$4) \quad W = K\, P_o\, A_o \cdot \sqrt{\frac{m}{2\pi\, k\, T_o}}$$

where K = Clausing's correction factor for orifice plate thickness

P_o = Pressure upstream of the orifice

A_o = Area of the orifice

T_o = Temperature of gas upstream of the orifice

Hence, the pumping speed can be obtained from

$$5) \quad Q_p = K \frac{P_o}{P_p} \cdot A_o \sqrt{\frac{k T_p}{2\pi m} \cdot \frac{T_p}{T_o}}$$

We assumed that

$$T_p = T_o = T = 530^{\circ}R$$

and reduced (5) to:

$$6) \quad Q_p = K \frac{P_o}{P_p} \cdot A_o \sqrt{\frac{k T}{2\pi m}}$$

Thus, measurement of P_o and P_p enables us to determine the pumping speed.

In the experiments, prior to the beginning of each run the chamber was permitted to reach an ultimate pressure which was generally below about 5×10^{-9} torr. All ion gages were outgassed and background pressure readings recorded. Then a constant mass flow rate of gas was introduced through one of the gas input plenum chambers (Figure 4). The flow was controlled by a Granville-Phillips metering valve (V_1 or V_2 in Figure 3). A steady-state pressure was established in the chamber almost immediately and pressure and flow rate measurements were made. Then the flow rate was increased, a new steady-state pressure reached, and another set of readings taken. The process was repeated until measurements over the entire pressure range of interest (up to about 10^{-3} torr) were completed. In the reduction of the data, the background pressure reading on each gage prior to the admission of the steady-flow rate of nitrogen was subtracted from subsequent readings taken while gas flowed into the chamber. This practice was based on the reasoning that we desired to measure only the contribution to pressure of the nitrogen bled into the system. In most cases the correction on the measured pressure was small for pressures greater than 10^{-8} torr.

The experimentally determined pumping speed of the array is shown as a function of the upstream pressure in Figure 12. The method by which the mass flow rate, W, was measured is indicated by the key on the figure. The values of P1 and P6 at a particular flow rate agreed fairly well over the entire pressure range, which indicates that the flow into the array was uniform. Both the pressure upstream of the array and the pumping speed shown in Figure 12 are based on the measurements made with gage P1.

In Appendix D an estimate of the uncertainty intervals associated with ion gage readings and with measurement of mass flow rate by the displacement oil manometer technique and by the orifice technique, are made. These estimates suggest that the pumping speed, when based on the mass flow indicated by the displacement oil manometer, would have an uncertainty interval of about $\pm$ 42 percent. When the orifice technique is used, the uncertainty interval would be about $\pm$ 57 percent.

The data show the pumping speed to be essentially constant at pressures below 5×10^{-6} torr. At pressures higher than 10^{-4} torr, the pumping speed increases rapidly with pressure. At a pressure level of 5×10^{-4} torr, the mean-free path of nitrogen equals the spacing between the chevrons. As this pressure is approached, the flow begins to depart from free molecular; the increase in pumping speed at higher pressures is associated with this departure. As the flow becomes more like a continuum flow, mass motion becomes appreciable, and higher pumping speeds result.

Tests made early in the experimental program indicated that the presence of condensate on the 20 K condenser had little effect on the pumping speed. The ion gages used for pressure measurement had not been calibrated so that the data obtained did not yield absolute values of the pumping speed. However, the data were quite reproducible and enable valid comparisons of results from one test to the next. The results of the early tests are shown in Figure 13. In order to avoid confusion we plot only a "relative pumping speed", with no absolute value.

In these tests, all mass flow determinations were made with the orifice technique. In tests No. 1, 2 and 3 all cryogenic surfaces were at operating temperatures and initially free of deposits. Test No. 4 was run after about 3 lbs. of nitrogen had been deposited on the condenser (by introducing a mass flow input to the chamber of about 1.5 lb/hr. for two hours). The frost deposit was readily visible to the naked eye and appeared as a smooth white coating on the condenser. As may be seen from the data, the presence of the deposit had little effect on the pumping speed. In Test No. 5 the chevron shields were uncooled; the condenser was thoroughly clean. Again, no substantial difference in pumping speed was observable from the data.

During pumping speed measurements at very low pressure the condenser was always maintained at or below 20 K. In one test the effect of condenser temperature on the pressure upstream of the array and the pumping speed was clearly demonstrated. With a constant input mass flow rate of 4.1×10^{-4} scc/sec., the condenser temperature was varied from 19 to 25 K. Data points for the increase in pressure (Δ P1) indicated by gage P1 and the pumping speed based on its indication are plotted against condenser temperature in Figure 14. The figure shows that as the condenser temperature was increased above 21 K, the upstream pressure began to rise and the pumping speed began to drop.

The solid curves shown in the figure were calculated. We would expect the increment in the pressure sensed by P1 due to the vapor pressure of the solid, P_v, at the condenser temperature, T_2, to be equal to

$$P_v \sqrt{\frac{T_p}{T_2}} ,$$

where T_p is the probe temperature. The probe will indicate a pressure increment higher than the vapor pressure because of the transpiration effect. The solid curve in Figure 14 marked $P_v \sqrt{\frac{T_p}{T_2}}$ was calculated from solid vapor pressure data[7]; we assumed that T_p = 530 R. Then, the calculated increment in upstream pressure, together with the measured upstream pressure corresponding to a condenser temperature less than 20 K (4.2×10^{-5} torr) was used to compute the pumping speed versus condenser temperature curve. The close agreement between calculated and experimental results shows that the effect of condenser temperature on performance is readily predictable.

C. ARRAY CAPTURE PROBABILITY AND CONDENSER STICKING COEFFICIENT

The capture probability, G_a, is a more basic property of the array than its pumping speed. The pumping speed depends on the definition of an upstream density or pressure. When G_a is close to unity, the molecular flux into the array can greatly exceed that rebounding from the array and the gas upstream of its inlet differs considerably from an "equilibrium" gas. Usual definitions of pressure and density are not very useful under these conditions. For that reason we used the density sensed by an open-ended probe with a particular inlet orientation (opening pointing across the flow) in our definition of pumping speed (Equation 1). This complexity of definition can be avoided if we use the capture probability to describe the pumping effectiveness of the array.

In Appendix A, the pressures upstream of a planar cryopumping array that would be indicated by an open-ended probe with various inlet orientations

are related to the mass flow rate, the probe temperature and the capture probability. An expression is also developed which relates the pumping speed to the capture probability. The analysis is based on the free molecular flow from a planar gas source to a parallel planar sink. The conditions in the experiments can be likened to the simple case analyzed in Appendix A if we think of the chevron inlet plane as a pumping plane, and the flow distributing screens as a planar gas source, both with areas equal to the cross sectional area of the cylindrical tank (see Figure 4). Then the inlet to the ion gages P1 and P6, are positioned similarly to that of the probe in Case B, Appendix A and the pumping speed, based on the upstream gas density sensed by P1 or P6, is related to the capture probability of the pumping plane, G_{pp}, by

$$7) \quad \frac{Q_p}{A_{pp}} = \frac{2\,G_{pp}}{2 - G_{pp}} \sqrt{\frac{k\,T_p}{2\pi\,m}}$$

where G_{pp} is the capture probability of the pumping plane and A_{pp} is the area of the pumping plane. The capture probability of the array alone, G_a, is simply related to the capture probability of the pumping plane by

$$8) \quad G_a = G_{pp} \times \frac{A_{pp}}{A_a}$$

where A_a = array inlet area. The cross section area of the tank, A_{pp}, equals 7.07 square feet, and the inlet area to the array, A_a, equals 3.25 square feet, so that $\frac{A_{pp}}{A_a} = 2.17$.

Perhaps the most basic quantity relating to the condensation process is the sticking coefficient, f, of the condenser. In Appendix B, a relationship is derived which relates G_a, the array capture probability to g_1, the probability that a molecule impinging on the chevrons shield would pass through without rebounding, g_2, the percent open area of the condenser, and f the sticking coefficient of the 20 K condenser. In the experimental array g_1 equals 0.23[8] and g_2 equals 0.25. For these values the capture probability is related to the sticking coefficient, as shown by Figure 15. Thus, Equations 7 and 8 and Figure 15 relate the experimentally determined pumping speed to the array capture probability and the condenser sticking coefficient. Capture probabilities and pumping speeds corresponding to values of f from 0.4 to 1.0 are tabulated below:

TABLE I

CALCULATED EFFECT OF CONDENSER STICKING COEFFICIENT ON THE EXPERIMENTALLY DETERMINED PUMPING SPEED FOR N_2

f	G	G_{pp}	$\frac{2\,G_{pp}}{2-G_{pp}}$	$\frac{Q_p}{A_{tank}}$ - CFS/ft^2	Q_p - CFS	$\frac{Q_p}{A_{array}}$ - CFS/ft^2
0.4	.177	.0814	.0848	32.9	232	71.4
0.5	.190	.0873	.0913	35.4	249	76.6
0.6	.200	.0920	.0965	37.4	263	80.9
0.7	.209	.0961	.1010	39.2	276	84.9
0.8	.216	.0993	.1045	40.5	285	87.7
0.9	.222	.1020	.1075	41.7	293	90.2
1.0	.226	.1040	.1098	42.6	300	92.3

Comparison of the pumping speed values in the table to the experimental results, Figure 12, establishes a range of array capture probabilities and condenser sticking coefficients. In Figure 12 most of the pumping speed data points below a pressure of 5×10^{-6} torr, fall between 232 and 276 cfs corresponding to sticking coefficients, f, of between 0.4 and 0.7 (as shown in Figure 12), capture probabilities, G, of between 0.177 and 0.209, and pumping speeds per unit area of array of between 71.4 and 84.9 cu. ft./sec./ft^2.

It is appropriate to note here the variations in the pressure indicated by an open-ended probe upstream of a planar array of large extent, that can be caused by the orientation of the probe inlet. From Equations (5) (6) and (7) of Appendix A we see that for a given mass flow rate and probe temperature, P_p is proportional to the factors listed below:

Inlet Orientation	P_p Proportional to this factor	Value of factor for $G_a = 0.2$
Upstream	$\frac{1}{G_a}$	5.00
Across the flow	$\frac{2 - G_a}{2 G_a}$	4.50
Downstream	$\frac{1 - G_a}{G_a}$	4.00

Thus, when G_a is relatively low, as it was in our experiments with nitrogen, the influence of probe orientation on indicated pressure would not be great. As G_a approaches unity the influence becomes more pronounced.

V. CRYOPUMPING OF CARBON DIOXIDE

A. GENERAL

The vapor pressure of CO_2 at 77 K is about 1.5×10^{-8} torr[7]. At any higher pressure it would be cryopumped on the chevrons. Pumping rates and capture probabilities for CO_2 should be typical of those attainable with gases that would be cryopumped on the chevrons. High rates are expected due to the unimpeded gas flow to the chevrons.

B. EFFECT OF SOLID DEPOSIT AND PRESSURE LEVEL ON PUMPING RATE

Tests made early in the experimental program suggested that a high pumping speed for CO_2 was not developed until a certain amount of deposit had formed on the chevrons. Quantitative measurements of this phenomena were later made in two tests.

The first test consisted of two runs. In the first run, the chamber was pumped to the low 10^{-9} torr range, with the diffusion pumps running and with the 20 K condenser and the liquid-nitrogen cooled surfaces at operating temperatures. No deposit was present on the chevrons at the start. The pumping speed for CO_2 was measured (in the same way as in the N_2 tests, Section IV-B) over the pressure range of 10^{-8} to about 4×10^{-6} torr. By running the test with the diffusion pumps and the 20 K condenser operative, we avoided any accumulation of gases non-condensable at the chevron temperature (77 K). The data obtained from this run is shown in Figure 16 (Run #1). Both the orifice technique and the displacement oil manometer technique were used to measure the mass flow rate as indicated on the figure. The pressure upstream of the array was measured by gage P1. As can be seem from the figure, the pumping speeds were of the same order of magnitude as those obtained with nitrogen until higher pressures were reached and it appears that CO_2 was not effectively pumped by the chevrons. After the run, a flow rate of CO_2 was admitted to the tank for a period of five minutes to form a further deposit on the chevrons. The CO_2 flow was stopped and the tank allowed to come to its ultimate vacuum.

With the deposit on the chevrons, the ultimate vacuum was only about 2.2×10^{-8} torr as measured by P1, a level slightly higher than the vapor pressure of CO_2 at 77 K (1.5×10^{-8} torr). One would expect the pressure indicated by P1 to be higher than the vapor pressure because of the transpiration effect associated with the warm (room temperature) gage. A second run was now made to determine pumping speed versus pressure as in the first run. The data, shown in Figure 16 (Run #2), clearly indicate the effect of pressure level on pumping speed. The pumping speed goes from 0 at the vapor pressure of CO_2 to very high values at pressures greater than 10^{-7} torr. With no gas input, the chamber was

at the vapor pressure; the absolute evaporation rate from the solid deposit exactly equaled the absolute condensation rate of the gas and the net pumping speed was 0. As gas flow was introduced, the pressure in the chamber exceeded the vapor pressure, the rate of condensation exceeded the rate of evaporation, and cryopumping commenced. The pumping speeds observed in this run were much higher than those observed in the run without deposit on the chevrons and we are let to the conclusion that high pumping speeds are developed only after a substantial deposit is formed on the condensing surface. This conclusion was given further credence by the next test.

The second test was begun with the chevrons free of deposit. A CO_2 flowrate of 0.15 scc/sec. was initiated; the pressure in the chamber was 6×10^{-6} torr as indicated by a nude ion gage in the same axial plane as P1 and P6 (see Section III-E). The flow rate was held constant and the pressure upstream of the array was monitored as a function of time. The results are shown in Figure 17, a plot of the pressure indicated by the gage versus time. The data show the effect of deposit thickness on the pumping rate for CO_2, since the deposit thickness can be considered proportional to the time scale. After about eight minutes, the pressure decreased rapidly to a level of about 1.5×10^{-6} torr and remained fairly steady at that level for the remainder of the test.

C. EFFECT OF PROBE INLET ORIENTATION ON INDICATED PRESSURE

With CO_2 being cryopumped by the chevrons, we would expect a high capture probability and a strong departure from equilibrium gas conditions upstream of the array. This situation is ideal for observing the effect of probe inlet orientation on pressure indication because the effect should be rather pronounced. To investigate the effect, the directional probes shown in Figure 18 were fitted on to P1 and P6. The tubes fitted snugly into the ion gage inlets to prevent leakage. The opening in the probe on P1 pointed upstream; that on P6 pointed downstream. The probes were made of stainless steel and were thoroughly cleaned on the inside to minimize the effect of outgassing on the pressure indications. Before the test, the chevrons were coated with a 0.7 gm CO_2 deposit. The chamber was permitted to reach its ultimate vacuum and the run was commenced. The pressures indicated by P1 and P6 with their directional probes, are shown in Figure 19, a plot of pressure versus CO_2 mass flow rate. The difference between the pressure indicated by the probe with its inlet pointed upstream and that with its inlet pointed downstream, is readily observable. The fact that the ratio of these two pressures at levels above 10^{-6} torr exceeds 10, shows the extreme importance of the orientation of the gage inlet.

D. ARRAY CAPTURE PROBABILITY

The results of the test with directional probes can be used to estimate the capture probability of the array for CO_2. We make use of the expressions relating the pressures indicated by an open-ended probe, with various inlet orientations, to the array capture probability, derived in Appendix A. As in our discussion of the results of the tests with nitrogen, we consider the flow distribution screens as a source plane, and the plane in which the edges of the chevrons lie as a sink plane. As can be seen in Figure 18, the inlets to the probes on P1 and P6 were approximately in the middle of the tank. Hence, these probes sense the local mass fluxes immediately upstream of the center of the array. The fact that the array does not fill the entire cross section of the tank should have relatively little influence on these local mass fluxes. Thus, the mass fluxes sensed by the probes on P1 and P6 should be those associated with the capture probability of the array proper rather than with the capture probability of the pumping plane. The pressure sensed by the probe with its inlet pointed upstream is related to the mass flux and the array capture probability by the following equation:

$$9) \quad (P_p)_A = \sqrt{\frac{2\pi k (T_p)_A}{m}} \cdot \frac{W}{A} \cdot \frac{1}{G_a}$$

The pressure indicated by the probe with its inlet pointed downstream is given by:

$$10) \quad (P_p)_c = \sqrt{\frac{2\pi k (T_p)_c}{m}} \cdot \frac{W}{A} \cdot \frac{1 - G_a}{G_a}$$

The equations may be combined to yield:

$$11) \quad G_a = 1 - \frac{(P_p)_c}{(P_p)_A} \cdot \sqrt{\frac{(T_p)_A}{(T_p)_c}}$$

The temperatures and pressures in the vicinity of the openings of the probes on gages P1 and P6 should be used in the equations. These temperatures were not measured. We can only surmise that they were somewhere between room temperature and 77 K, and because both probes had the same geometry, that their temperatures at similar points were about the same. The pressures indicated by the ion gages would differ from those existing inside the probe near the opening, due to the thermal transpiration effect in the probe tube. But for probes with similar

temperature distributions we would expect that the ratio of gage readings, P6/P1, would equal the ratio $(P_p)_c / (P_p)_A$.

By this reasoning

$$G_a = 1 - \frac{P6}{P1}$$

With this equation and the measured values, P6 and P1, the capture probability of the array for CO_2 may be computed. The results are tabulated below as a function of the pressure indicated by the probe whose inlet was pointed upstream.

TABLE II - Array Capture Probability for CO_2

Probe Pressure, Inlet Upstream, P1 - torr	Array Capture Probability for CO_2, G_a
4.6×10^{-7}	0.70
1.2×10^{-6}	0.75
3.1×10^{-6}	0.74
1.3×10^{-5}	0.92
2.0×10^{-5}	0.94
6.8×10^{-5}	0.93

The actual CO_2 sticking coefficient on the chevrons surfaces would be less than the capture probability of the array because the chevron geometry is such as to cause a molecule to experience multiple bounces before its return to the vacuum space upstream of the array.

From the observations with CO_2 it seems likely that very high capture probabilities will be exhibited for gases that will be cryopumped by the chevrons.

E. VAPOR PRESSURE LIMITATION

If the chevrons are maintained at 77 K, CO_2 will be cryopumped by them at any pressure greater than about 1.5×10^{-8} torr. In certain instances, this may prove to be a disadvantage. For example, consider a chamber under test in which, from time to time, high partial pressures of CO_2 occur so that deposits would form on the chevrons. Even if all other gas inputs to the chamber were eliminated subsequent to the deposition of CO_2, the pressure level in the chamber could not be brought below 1.5×10^{-8} torr until all the CO_2 deposits were evaporated. In time, the CO_2 would evaporate from the liquid-nitrogen cooled chevrons and be re-deposited on the 20 K condenser, but the rate of this evaporation and re-condensation would be very low. It would, in fact, correspond to the number of molecules striking a unit area of surface per unit time from an equilibrium gas cloud of CO_2 at 77 K and at the vapor pressure corresponding to the temperature (1.5×10^{-8} torr). If the CO_2 had been deposited at a rate corresponding to a partial pressure in the chamber of about 10^{-5} torr, it would take approximately six hundred times as long for the solid on the chevrons to evaporate as it did to accumulate.

The situation can be avoided, by operating the chevrons at a high enough temperature to prevent the cryopumping of CO_2 at partial pressures commonly encountered in the chamber. At 98 K the vapor pressure of CO_2 is 10^{-4} torr. Thus, operation of the chevrons at that level would prevent CO_2 from being cryopumped at any pressure below 10^{-4} torr. It would, of course, be cryopumped by the 20 K condenser. Although the rate of CO_2 removal would be substantially reduced from that which might be achieved by cryopumping on the chevrons, the ultimate pressure attainable subsequently would not be limited to the 1.5×10^{-8} torr level. In short, in tests where it is likely that substantial amounts of CO_2 might be sporadically given off by the test object, and where the chamber must be operated for most of the tests at pressures below 10^{-8} torr, it would be desirable to avoid cryopumping the CO_2 on the chevrons.

VI. NON-CONDENSABLE REMOVAL (H_2)

At 20 K, hydrogen and neon have high vapor pressures (760 and 35 torr respectively) and helium will not even condense. Because these gases will not be cryopumped at the 20 K level; they are often called non-condensables. Of the three, perhaps hydrogen is the most common one in ultra-high vacuum systems. Although hydrogen is not simply condensed at the low operating pressures of interest here, recent investigations have suggested that it may be adsorbed or trapped by other impurities frozen out on a surface at temperatures between 8 and 20 K[9]. In order to gain some insight into this possibility and to establish the relative pumping speed of our experimental apparatus for non-condensables, several tests were run in which hydrogen was bled into the chamber and measurements similar to those made in the nitrogen pumping speed tests were carried out.

The diffusion pumping system described in Section III-E, was included primarily for the removal of non-condensables. Its speed for gases admitted upstream of the chevrons was considerably reduced because of the restrictions imposed by the chevrons, the condenser, the back shields, the 90° elbow and the LN_2 cooled trap. As may be seen in Figure 4, the flow from the gas input point to the inlet of the 90° elbow was rather tortuous. This situation was peculiar to our set-up, in particular to the arrangement of back shields used in our apparatus. It need not exist in other chambers.

In the first test, with the diffusion pumps running, the chevrons, back shields and outer shields were cooled with LN_2 to 77 K, but the condenser was not cooled by helium gas flow. Consequently, the temperature of the condenser probably reached a level in the vicinity of 100 K by radiation cooling. With these conditions the ultimate pressure achievable was only about 10^{-6} torr. Measurements of the pumping speed for hydrogen versus pressure led to the data indicated by the circles in Figure 20. The pumping speed shown by this data is indicative of the speed of the diffusion pumping system as restricted by the array. Next, a test was conducted in which the condenser was held at a temperature below 13 K. During this run the pressure in the chamber was unsteady. However, readings were taken and the data shown by the squares in Figure 20 is based on these readings. In a subsequent run, with the condenser at 20 K, the pressure readings were so unsteady that it was not possible to obtain meaningful data. Consequently, a run with the condenser at 30 K was carried out. The pressure readings in this final run were quite steady and led to the data shown by the triangles in Figure 20.

It is interesting to note that Brackman and Fite[9] observed a rapid increase in the adsorption of hydrogen by frozen water vapor, nitrogen and oxygen, as the temperature of the cold surface was lowered below 20 K. It is entirely possible that the unsteady pressure readings observed in our test run with the condenser at that temperature level were caused by this phenomena. It was beyond the scope of this investigation to experiment further with adsorption or trapping of hydrogen.

The test apparatus had been designed so that the pumping speed for hydrogen would be much less than that for nitrogen or CO_2 and Figure 20 shows that such was the case. During pumping speed tests with nitrogen and CO_2 it was desirable to maintain the diffusion pumping system in operation. In this way non-condensables introduced into the chamber with the input gas were continuously removed and the build-up of their concentrations during the course of a pumping speed run was prevented. Accumulated non-condensables can interact with the condensable gas flow so as to complicate the determination of pumping speed[10][11]. Though a substantial pumping speed for non-condensables was continuously maintained, its magnitude was small compared to the speeds of the system when cryopumping nitrogen and CO_2, and thus the speeds determined for those gases could be attributed only to the effect of cryopumping.

VII. HEAT LOADS ON CRYOPANELS

The refrigeration requirements at 20 K and 77 to 100 K are dependent on the heat loads on the cryopanels at those two temperature levels. In a chamber wherein the walls are covered by cryopumping array, any heat input to the working space inside the array is absorbed at one of the two temperature levels. To minimize the cost of supplying refrigeration it will be desirable to absorb as much of the energy as possible at the 77 to 100 K level. The fraction of irradiation on the array which is transmitted to the condenser will often comprise the major part of the refrigeration load at 20 K; hence, it must be known if the 20 K refrigeration source is to be sized with confidence.

It is difficult to estimate the fraction of irradiation transmitted to the condenser by analytical methods for, in order to make such estimates, the surface radiation properties of the panels must be known. These properties can be measured in the laboratory under certain conditions[4] but evaluation of the surface radiation properties under actual operating conditions is extremely difficult. Our experimental heat load measurements were aimed at determining what percentage of incident irradiation will be transmitted to the 20 K condenser, during operation under typical conditions.

The quantity of primary interest is the fraction of incident irradiation which reaches the condenser, q_t/q_i. It is desirable to ascertain this fraction for both infrared and simulated solar irradiation and we have made measurements with the two sources described in Sections III-F and III-G. The amount of incident irradiation was determined by measuring the boil-off rate of liquid nitrogen from the coolant tubes in the chevrons, while the transmitted irradiation was determined from measurement of the heat load on the 20 K condenser. The condenser heat load was obtained from the measurement of the flow rate and the temperature rise of the helium gas which flowed through the condenser coolant tubes. Measurement of the low flow rates and small temperature rises associated with the extremely small heat loads on the condenser posed difficult problems and required the special instrumentation described in Section III-C.

Numerous difficulties were encountered in making the heat load measurements. Because they may be common in experiments of this type, it seems worthwhile mentioning them here. They included:

1) A high background heat load on the condenser caused by contact with the liquid-nitrogen shields.

2) A helium leak in the vacuum jacket of the helium calorimetric flowmeter which reduced the effectiveness of the high-vacuum insulation around the flowmeter and made good measurement of helium flow rate impossible.

3) Low heat input to the array from both the solar and infrared sources.

4) Difficulty in controlling and measuring liquid nitrogen boil-off from the combined chevron, back-shield circuit.

In early heat load measurement tests the background heat load on the condenser was about 5 watts. With this high background, the incremental loads associated with the introduction of solar or infrared irradiation could not be distinguished. The high background was largely caused by contact between the condenser and the liquid-nitrogen shield surrounding it. When this contact was eliminated by careful positioning (with stainless steel guy wires and appropriate jacking) of the condenser with respect to the liquid-nitrogen shields, the background heat load was reduced from 5 watts to about 1.5 watts.

The helium leak in the calorimetric flowmeter was located and repaired so that the effectiveness of the high-vacuum insulation was improved. Prior to its repair, the insulation produced by the best vacuum that could be attained (in the 1-micron range) was poor. As a result the background heat input to the calorimetric flowmeter was so large that accurate flowrate measurements were impossible.

In initial tests infrared irradiation was produced by warming the end of the tank upstream of the chevrons with heat lamps. An incremental heat load on the chevrons of only about 20 to 30 watts was produced and no significant change in the condenser heat load was observed. In later tests the IR source shown in Figure 10 was utilized. With this arrangement, an incremental heat load of 50 to 60 watts was obtained. The solar source shown in Figure 9 generated only enough output to impose a load of about 60 watts on the chevrons. The fraction of irradiation transmitted to the 20 K condenser was sufficiently small that with these power levels, the incremental heat load on the condenser was difficult to discern.

The difficulty in controlling the liquid-nitrogen flow to the chevron and back-shield circuit, stemmed from the necessity of maintaining the exhaust temperature slightly in excess of the boiling temperature so as to insure that no liquid was carried over from the chevrons into the exhaust warm-up tube. If carry-over occurred, vaporization of liquid in the warm-up tube would produce an apparent boil-off rate considerably in excess of the true boil-off rate. Our approach was to monitor the temperature in the exhaust line and to control the flow input to the shields so as to maintain the exhaust temperature at about 80-90 K. Precise control was found to be quite difficult, probably because of the two-phase flow in the coolant tubes.

Even though considerable effort was expended in refining heat load measurement techniques, accurate determinations of heat loads were not possible. However, data of a semi-quantitative nature was obtained which gives a good indication of the magnitude of the heat loads, which may be expected. The results of our best measurements are shown in Table III.

TABLE III - HEAT LOAD MEASUREMENTS

Test No.	Condensate Deposits	Background Loads		Total Loads With Infrared Energy on Array Inlet		Total Loads With Solar Energy on Chevrons	
		Chevrons, watts	Condenser, watts	Chevrons, watts	Condenser, watts	Chevrons, watts	Condenser, watts
1.	None	54	1.91				
2.	None	56	1.30	117	1.50	110	1.50
3.	1.3 gms H_2 2.5 gms CO_2	61	1.33	117	1.92	-	-
4.	1.3 gms H_2 2.4 gms CO_2	58	1.50	-	-	121	1.62

The vacuum in the chamber for all these tests was in the range of 10^{-8} torr, so that the heat transferred by gas conduction and convection was negligible. In Tests 1 and 2 no deposit was present on the cold surfaces other than that present in a normally clean tank. In Test 1 we measured only the background heat loads on the condenser and chevrons. In Test 2 the background was measured, then IR irradiation introduced, and the total chevron and condenser heat loads were re-measured. Next, the IR was removed, solar irradiation introduced, and the heat load measurements repeated. In Tests 3 and 4 we first deposited nitrogen on the 20 K condenser and CO_2 on the chevrons. The amounts of deposit are indicated in the Table. The entire front surface of the condenser was coated with N_2 deposit, easily visible to the naked eye. The CO_2 was deposited on the front surface of the chevrons and formed a white film, also easily seen by the naked eye. The background heat loads were measured after the condensate deposition. Then, the measurements with IR and solar irradiation were made. Total heat loads are shown in Table III. The values are averages of a number of measurements under the conditions indicated.

As can be seen from the tabulated condenser heat loads, in attempting to distinguish the influence of IR or solar irradiation, we are faced with the problem of detecting small changes in the condenser heat load. Fluctuations in the total condenser heat load and uncertainties in measurement may obscure the influence of irradiation. Therefore, it was necessary to try to establish the magnitude of the uncertainties in the observed condenser loads. Estimates of the uncertainty intervals to be expected from our experimental determinations are presented in Appendix C. In the Appendix the uncertainty intervals in the various quantities that were measured in the determination of the fraction of irradiation transmitted to the 20 K condenser are estimated and combined, by the methods of error analysis, to establish the uncertainty interval in the quantity q_t/q_i. The data from Table 1 and the uncertainty estimates from Appendix C were then combined to form Table IV.

The last row in Table IV, "Estimated maximum range of q_t/q_i", was established by adding and subtracting half of the uncertainty interval to and from the "Observed" values. Since the lower limit on q_t/q_i must be zero, negative lower limits were called zero.

1.65 percent of incident irradiation was transmitted in Test No. 3, in which IR irradiation impinged on the array and solid deposits were present on both the condenser and the chevrons. This is the highest percent transmitted, which can be deduced from any of the tests we have run. Even with substantial solid deposits, the chevrons continued to provide effective irradiation shielding. The higher maximum value of q_t/q_i for solar energy in Test No. 2, as compared to Test No. 4, seems unreasonable because we would expect the effective absorptivity of the chevrons for solar irradiation to be reduced by the deposit of CO_2. However, since we cannot ascertain where within the interval of uncertainty the true value of q_t/q_i lies, it is entirely possible (and from physical reasoning even likely) that the true value in Test No. 4 was greater than Test No. 2. In this regard, the statements of

TABLE IV

ESTIMATED HEAT LOAD LIMITS

Test Number		2	3	4
Observed Incremental IR Loads	Δq	.20	.59	---
	ΔQ	61	56	---
Observed Incremental Solar Loads	Δq	.20	---	.12
	ΔQ	54	---	63
Observed q_t/q_i	IR	.0033	.0105	---
	Solar	.0037	---	.0019
Estimated Uncertainty Interval of q_t/q_i	IR	.011 (±.0055)	.012 (±.006)	---
	Solar	.012 (±.006)	---	.011 (±.0055)
Estimated Maximum Range of q_t/q_i	IR	0-.0088	.0045-.0165	---
	Solar	0-.0097	---	0-.0074

maximum ranges presented in the Table may be somewhat misleading.

In summary, though the results presented in Table IV do not establish with much precision the values of q_t/q_i that may be expected, they do indicate a low transmission of irradiation to the condenser under a variety of conditions.

The background condenser heat load averaged about 1.5 watts. Based on measurements with the IR source (Test No. 2) up to about 0.5 watts of that amount can be accounted for by the transmission of heat radiation from the warm walls of the tank through the chevrons to the condenser. Therefore, about 1 watt must have been caused by:

1) Direct radiation from the chevrons and back shields.

2) Direct radiation from the outer shields.

3) Transmission of radiation from the warm walls of the tank through the openings in the back shields.

4) Conduction through piping and supports.

These items are all peculiar to our experimental set-up, and tend to make the total heat load on the condenser per unit of array inlet area, higher than those that may be achieved in larger installations.

VIII. RESIDUAL GAS COMPOSITION

Measurement of gas composition within the chamber was desirable for two main reasons.

1) It would indicate the residual gases in the chamber which limited the ultimate pressure while cryopumping.

2) It would provide useful information on the simultaneous pumping of two gases, a condensable and a non-condensable.

An Omegatron mass spectrometer was used for gas composition measurements. Useful results pertaining to the residual gas composition in the chamber, during cryopumping, were obtained, but available funds were exhausted before we were able to make measurements during the simultaneous pumping of two gases.

The Omegatron unit was described in Section III-D. As pointed out, the Omegatron tube and an ion gage (P2) were teed to a common tubulation; the tubulation had its inlet adjacent to the 20 K condenser, inside the LN_2 cooled radiation shields (Figures 3 and 4).

The time available for testing with the Omegatron was extremely limited so that only some semi-quantitative results were obtained with the device. Calibrations were attempted with both nitrogen and hydrogen; a rough calibration for nitrogen was obtained but the calibration results for hydrogen were anomalous. The best determinations that we could make indicated that for nitrogen the sensitivity factor, S, as defined by the equation below

$$S = \frac{I_+}{P I_-}$$

where I_+ = Ion current

I_- = Electron current

P = Pressure in tube

was 35 $torr^{-1}$.

The most useful data was obtained in a run made to determine what gases would be present after a rapid pump down from one atmosphere using both diffusion pumps and the cryopump. Starting with the tank at 1 atmosphere the chamber was roughed down to about 150 microns, the diffusion pumps were started, and cooldown of the condenser was begun. 200 minutes after initiation of rough down the

condenser had reached a temperature below 18 K. At that time all liquid-nitrogen surfaces were cooled to operating temperature. The pressure at 250 minutes from start was 1.2×10^{-8} torr (as indicated by P1). Bake-out of the Omegatron tube was begun; the glass was baked at a temperature of 400 to 500 F for three hours. The elements of the tube were warmed to a dull red with an RF heater for one hour to complete the bake-out. Nine hours after the initiation of pumpdown the Omegatron had been effectively out-baked and the chamber pressure had reached a level of 7.2×10^{-9} torr (again, as indicated by P1). The pressure indicated by P2 (teed to the Omegatron) was 5.5×10^{-9} torr. One would expect this pressure to be lower than the pressure upstream of the chevrons because of the proximity of the gage inlet to the condenser. The condenser is surrounded by liquid-nitrogen cooled surfaces so that condensables at 77 K, which might be present outside the liquid-nitrogen cooled shields, have been eliminated.

The results of the gas analysis at this time are as follows: The mass 2 peak was barely discernible. Based on the approximate nitrogen sensitivity noted above, corrected to apply to hydrogen, the partial pressure of hydrogen sampled by the Omegatron was about 4×10^{-10} torr. The mass 4 peak was not discernible. The major peaks occurred at mass numbers of 12, 14, 26, 28 and 32. The largest peak was at mass 28. If this had been due only to nitrogen, it would have corresponded to a partial pressure of about 5×10^{-9} torr. However, part of the peak may have been due to CO, for which the gage was not calibrated.

The major conclusion to be drawn from these results, is that the partial pressure of non-condensables under the conditions described, was very low. The pumping speed of the diffusion pumping system for hydrogen (Figure 20) was about 35 cu.ft./sec. Using the approximate hydrogen partial pressure from above, and this pumping speed, we estimate that the rate of hydrogen outgassing in the chamber was about 5×10^{-7} scc/sec. Possible sources of hydrogen are:

1. The walls of the chamber.
2. Aluminum cryogenic panels.
3. The flow distribution screens.
4. The breakdown of water vapor or hydrocarbons by the Omegatron.

Since the aluminum panels were being operated at liquid-nitrogen temperature during the analysis, their emission of hydrogen by outgassing should have been small. The amount of hydrogen generated by gas decomposition within an Omegatron tube is usually quite small also. The most probable sources of hydrogen outgassing were the metal chamber walls and flow distribution screens.

Considering the low partial pressure of hydrogen and the absence of a detectable amount of helium in the chamber, the pressure indicated by the ion gage connected to the Omegatron tubulation (5.5×10^{-9} torr) appears to be high. Since the inlet to the gage tubulation was adjacent to the 20 K condenser, as shown by Figure 4, it should have "seen" much lower partial pressures of nitrogen

and less volatile gases. This may have been due to the fact that our bake-out of the Omegatron tube was less thorough than that recommended for ultra-high vacuum measurements. The manufacturer recommends bake-out at 400 C for 12 hours followed by degassing of the metal elements at 750 C for two hours. It seems likely that the pressure level indicated by the Omegatron and the ion gage was due more to outgassing from the tubulation and the two gages, than to the presence of gases adjacent to the condenser.

BIBLIOGRAPHY

1. "Feasibility Studies and Facility Requirements for Large Scale Space Environment Facility - The Application of Cryogenic Techniques to the Problem of Simulating the Low Temperature and High Vacuum Characteristics of Space Environments" by Arthur D. Little, Inc., December 1, 1959. Report to Arnold Engineering Development Center, ARDC, USAF, Tullahoma, Tenn.

2. "Pressure Simulation of Outer Space", D. J. Santeler, Vacuum Technology Transactions, 1959, Pergamon Press.

3. Progress Reports to AEDC (this project) for periods ending September 15 and November 15, 1960.

4. Progress Reports to AEDC (this project) for period ending November 15, 1960.

5. Progress Reports to AEDC (this project) for periods ending April 15, May 15 and June 15, 1961.

6. Progress Report to AEDC (this project) for period ending September 15, 1960 and April 15, 1961.

7. "Vapor Pressure Data for Some Common Gases", R. E. Honig and H. O. Hook, RCA Review, September 1960.

8. "Optimization of Molecular Flow Conductance" L. L. Levenson, N. Milleron and D. H. Davis, Univ. of California Radiation Laboratory Report 6014.

9. "Condensation of Atomic and Molecular Hydrogen at Low Temperatures" - R. T. Brackman and W. L. Fite, January 30, 1961, General Atomics Division of General Dynamics Corp. Report (GA-1683) to Air Force Office of Scientific Research, AFOSR-TN-60-1246.

10. "General Cryopumping Study", E. S. J. Wong, J. A. Collins, Jr., and J. D. Haygood, August 1961 - Paper presented at 1961 Cryogenic Engineering Conference, Ann Arbor, Michigan.

11. "A Study of Cryopumping with Non-Condensable Removal", R. W. Moore, Jr., USCEC Rept. 83-205 (Univ. of So. Cal.) AFOSR 561, March 1961.

12. "Describing Uncertainties in Single-Sample Experiments", S. J. Kline, F. A. McClintock, Mechanical Engineering, January 1953.

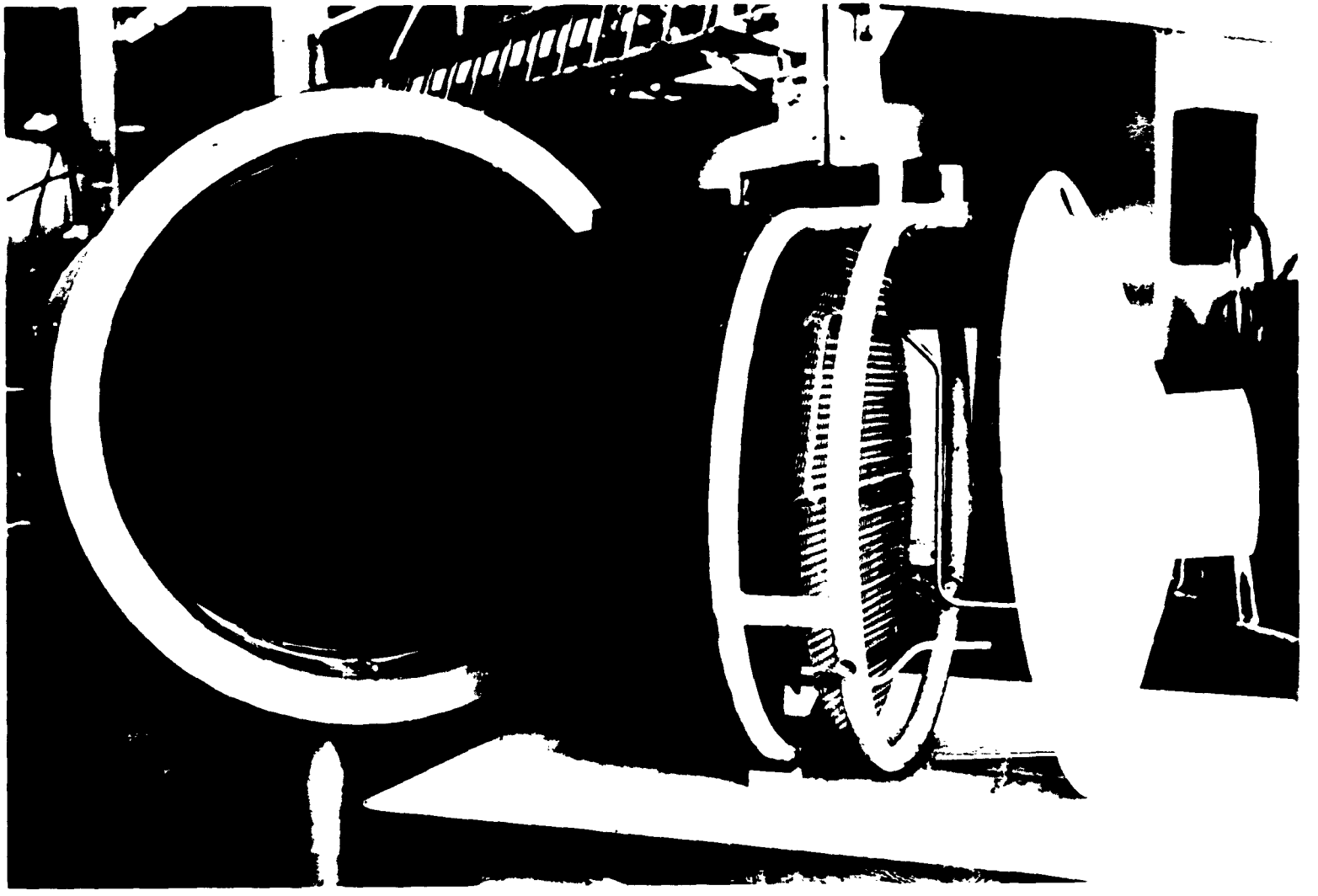

Figure 1 Experimental Cryo-Array – Welded Construction

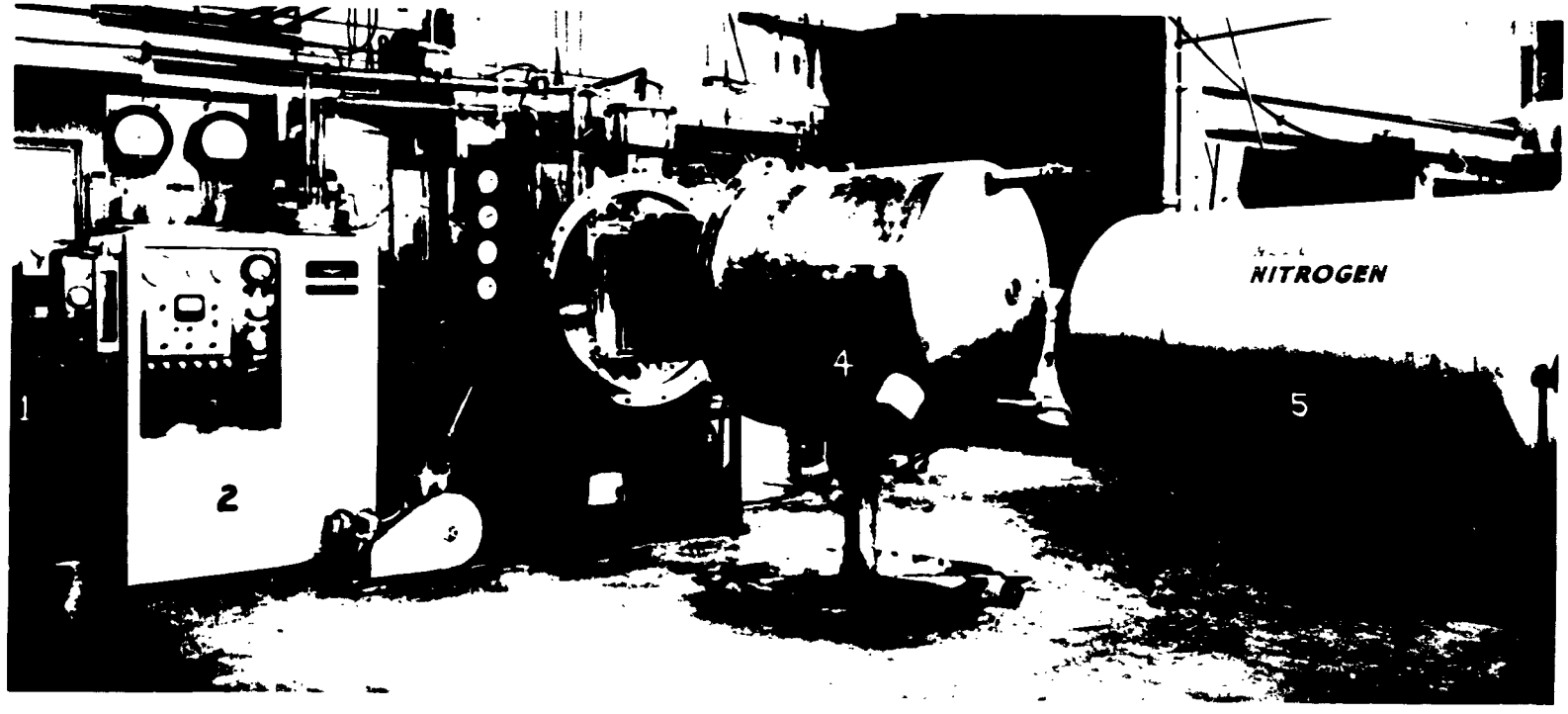

Figure 2 Test Set-Up – Over-all View

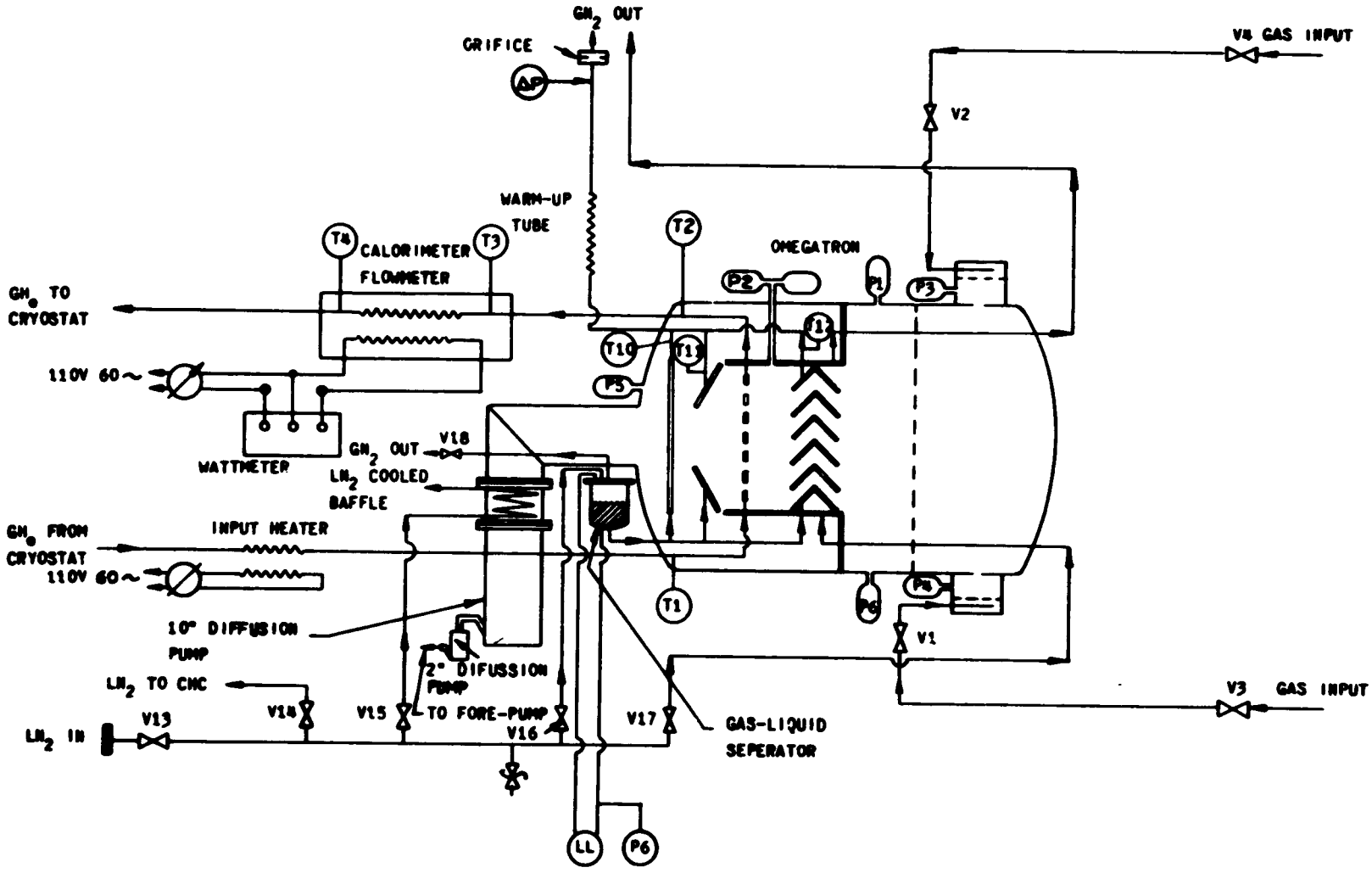

FIGURE 3 Flowsheet for Cryopumping Test System

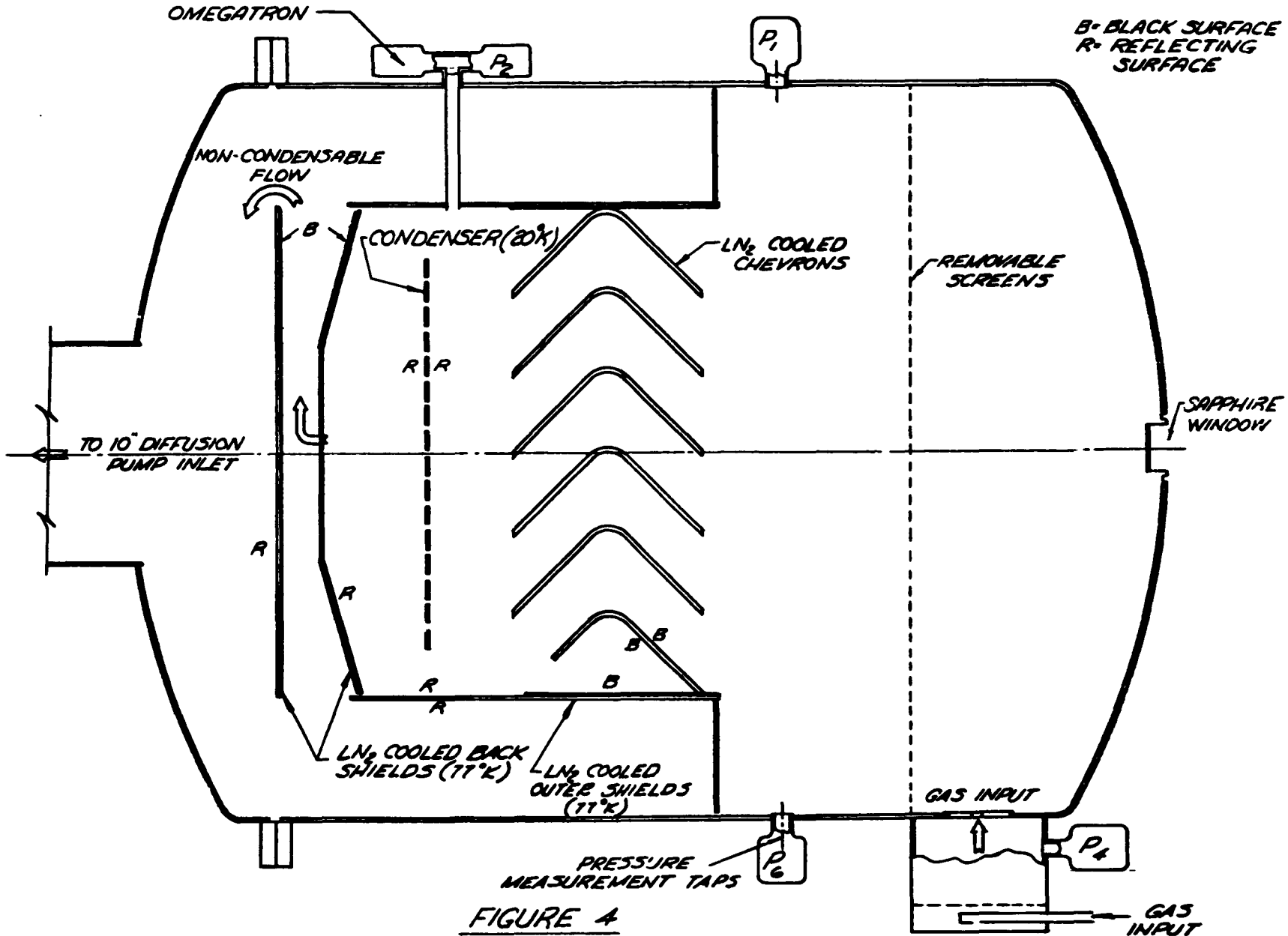

FIGURE 4
SCHEMATIC CROSS SECTION
OF CRYOPUMPING CHAMBER

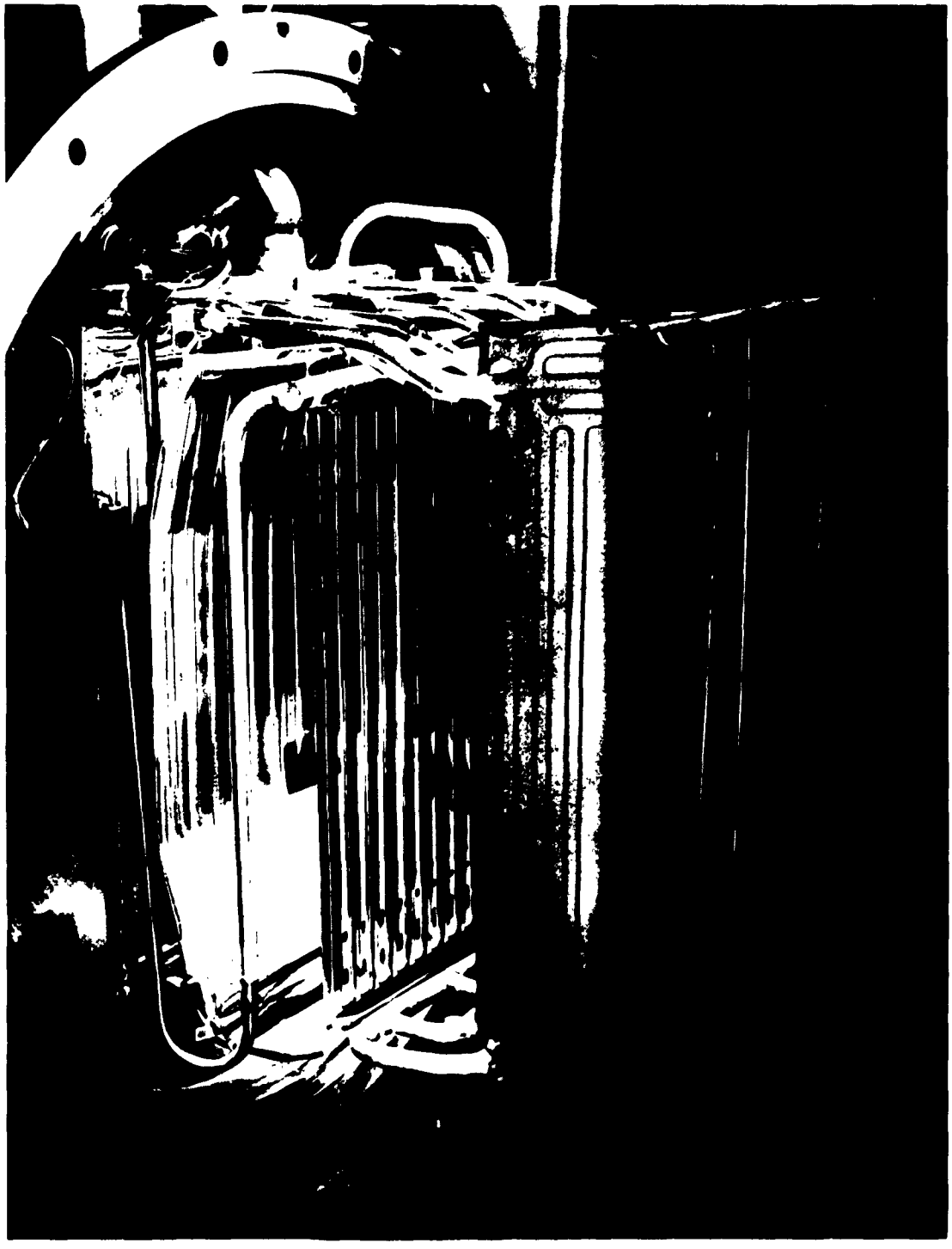

Figure 5 Experimental Cryo-Array – "Tubed Sheet" Construction

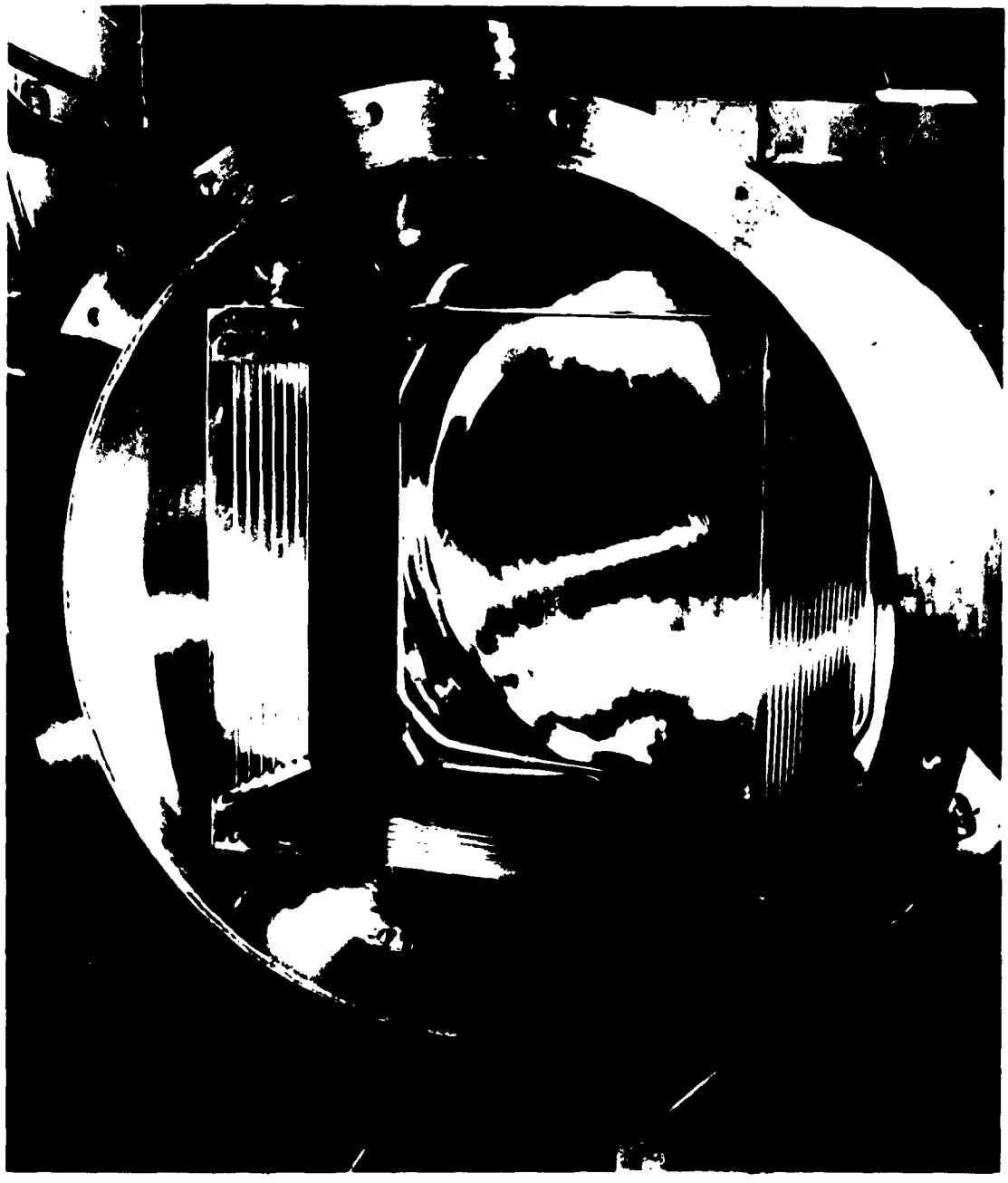

Figure 6 Vacuum Chamber with Outer Shields

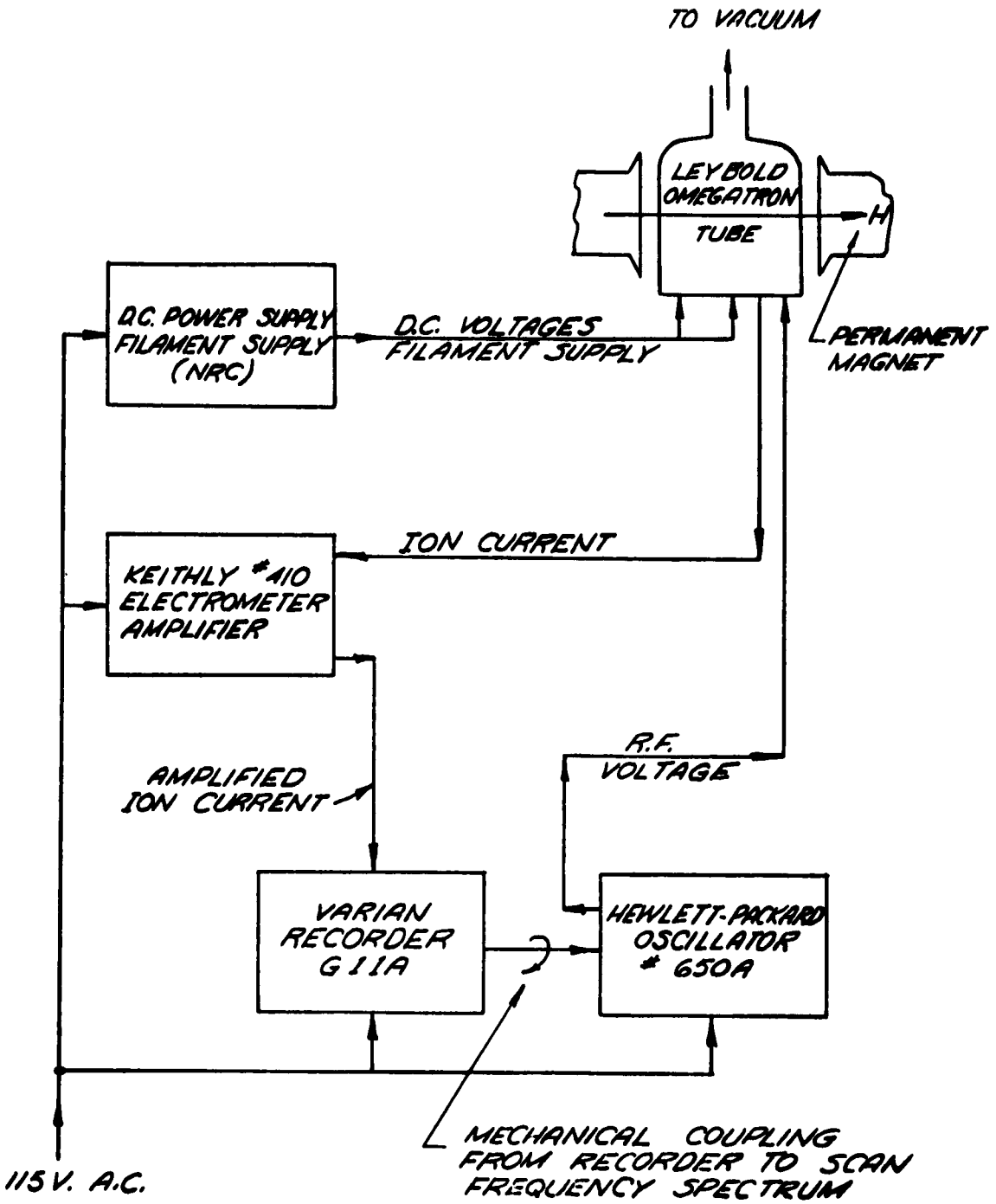

FIGURE 7
BLOCK DIAGRAM - OMEGATRON UNIT

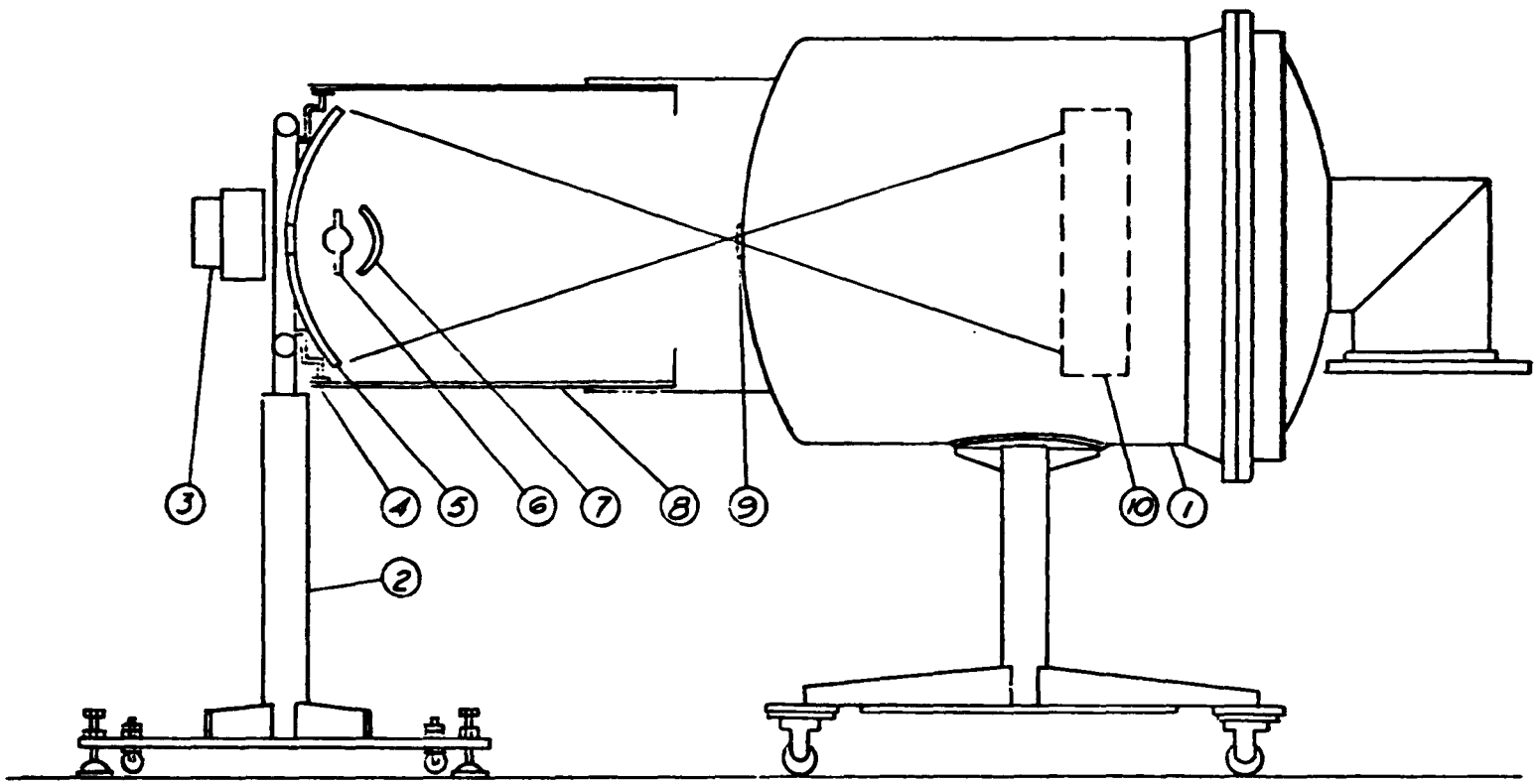

(1) VACUUM TANK
(2) OPTICAL STAND
(3) BLOWER
(4) REFLECTOR FRAME
(5) ELLIPTICAL MIRROR
(6) XENON - MERCURY LAMP
(7) SPHERICAL MIRROR
(8) HOOD
(9) SAPPHIRE WINDOW
(10) CHEVRONS

FIGURE 8
SOLAR SOURCE SET-UP

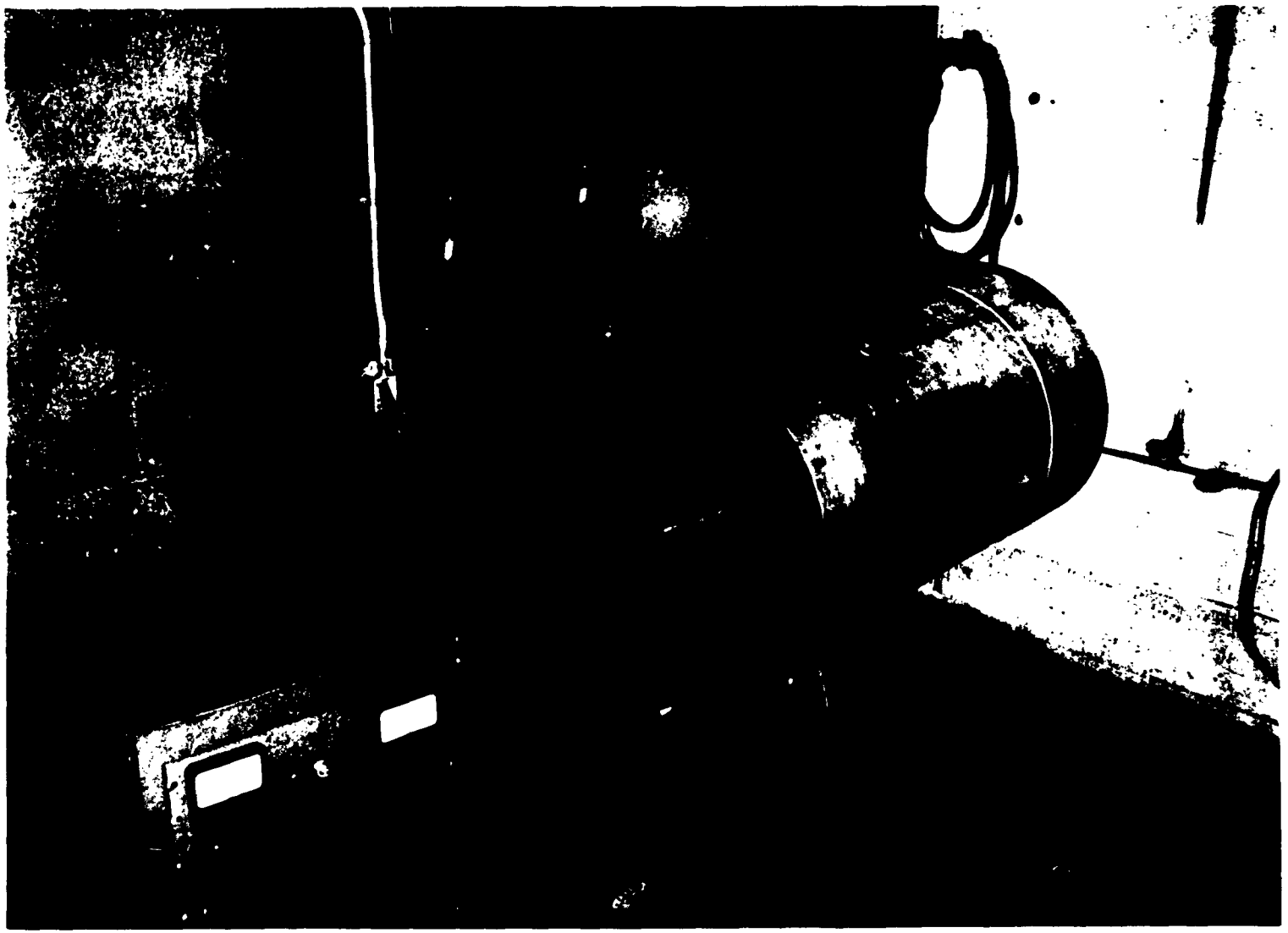

Figure 9 Solar Source Unit in Operation

Figure 10 IR Source in Tank

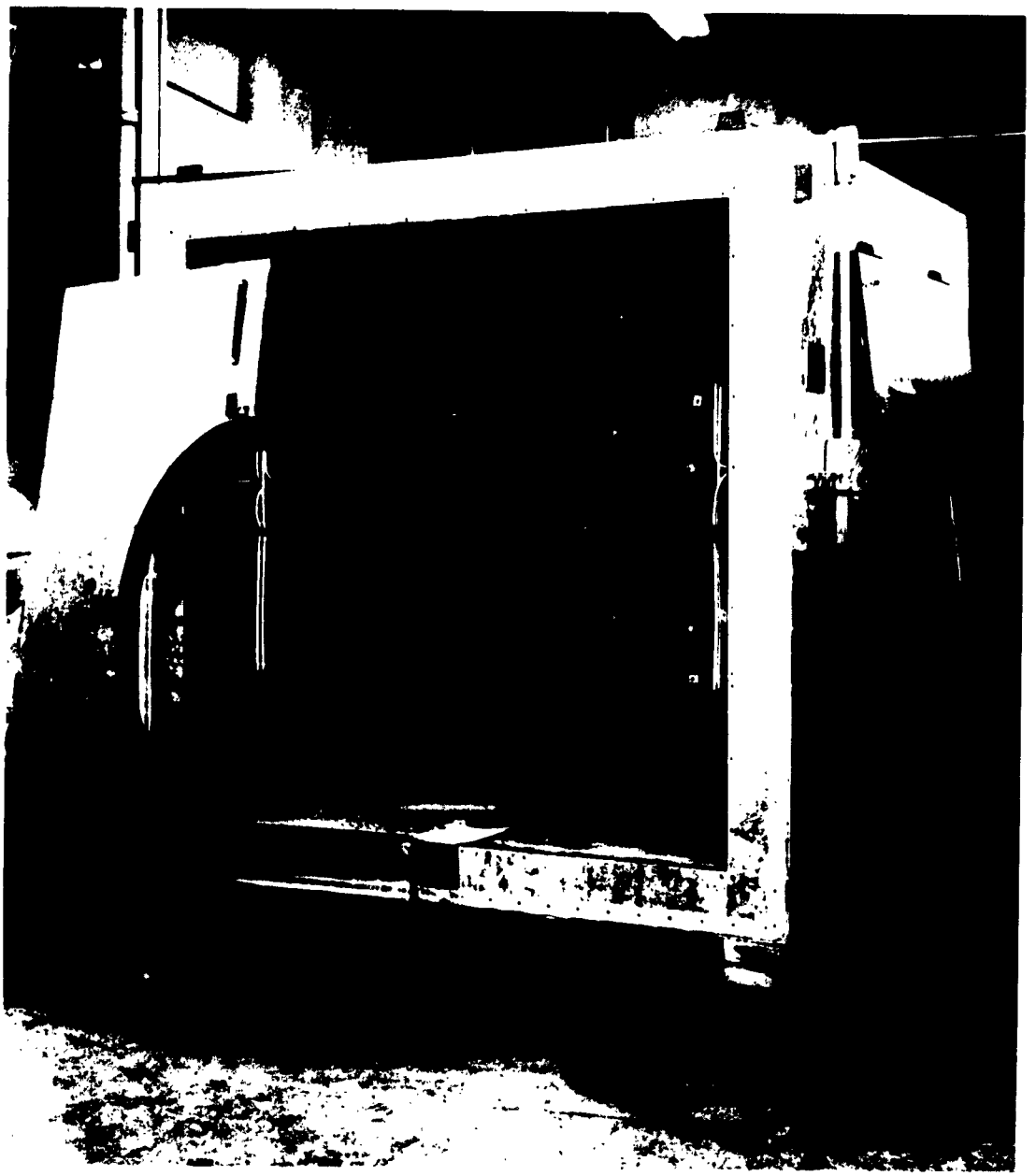

Figure 11 Bake-Out Oven

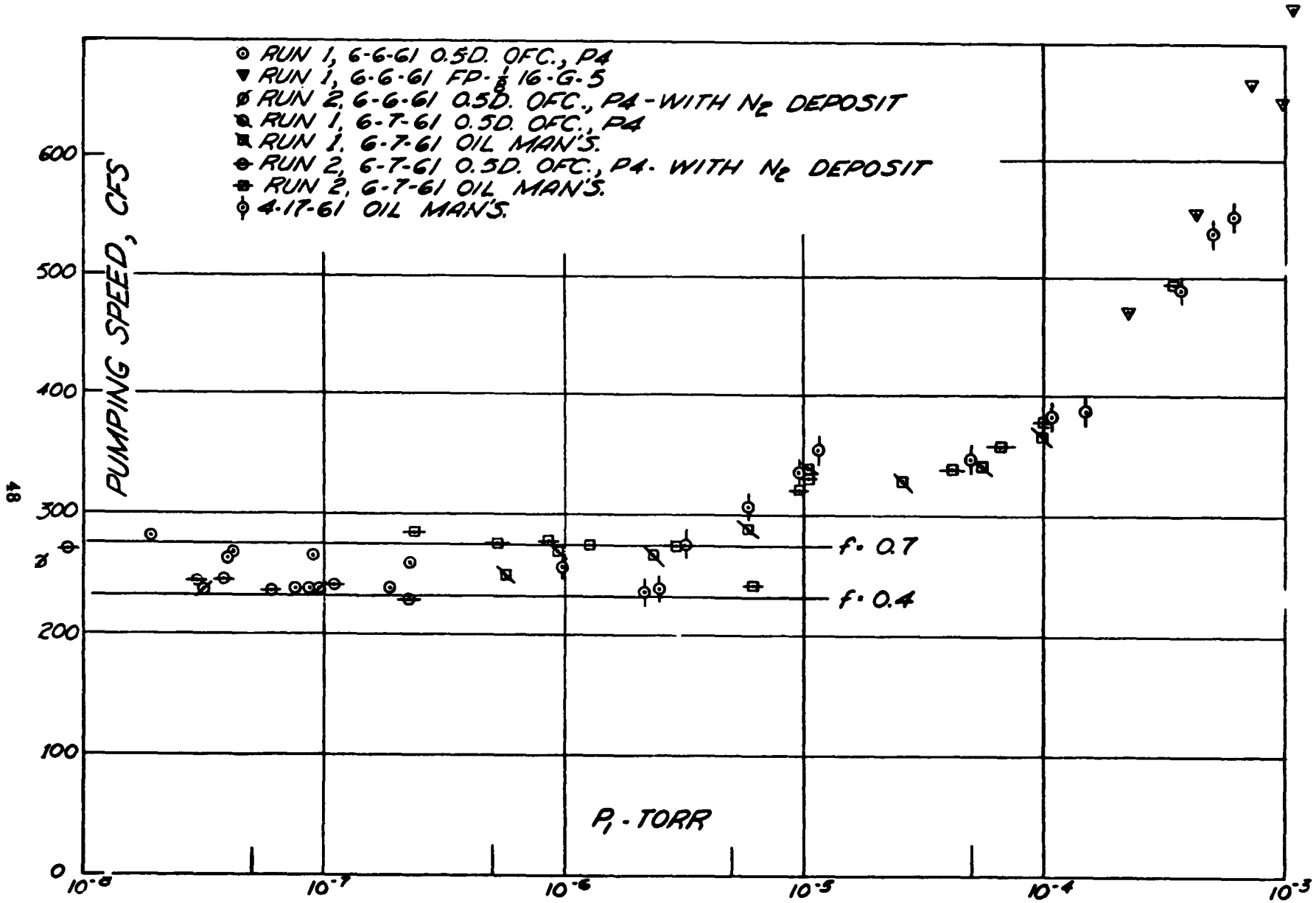

FIGURE 12
PUMPING SPEED FOR N_2

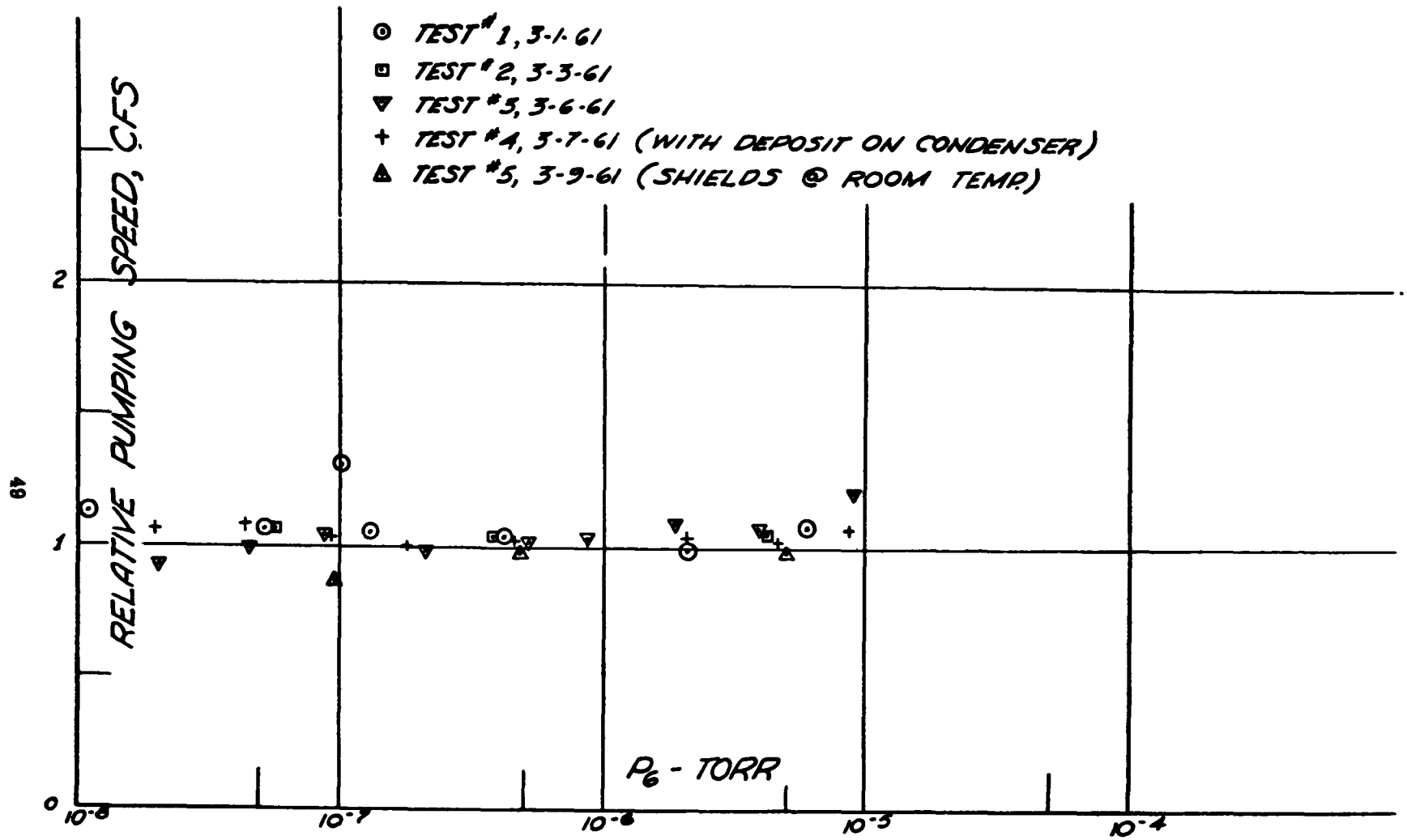

FIGURE 13
RELATIVE PUMPING SPEED FOR N_2
EFFECTS OF DEPOSIT AND CHEVRON TEMPERATURE

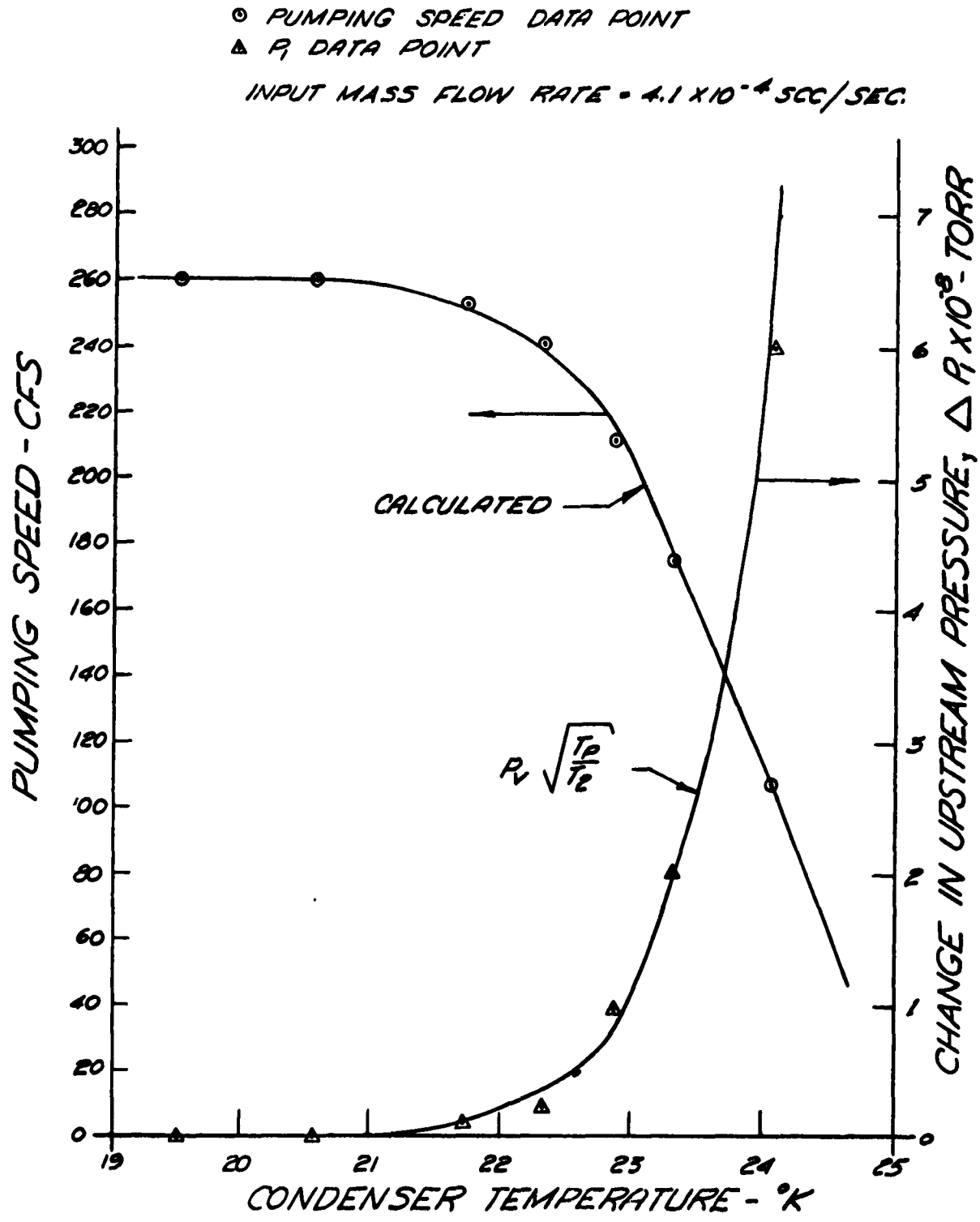

FIGURE 14. EFFECT OF CONDENSER TEMPERATURE ON UPSTREAM PRESSURE & PUMPING SPEED.

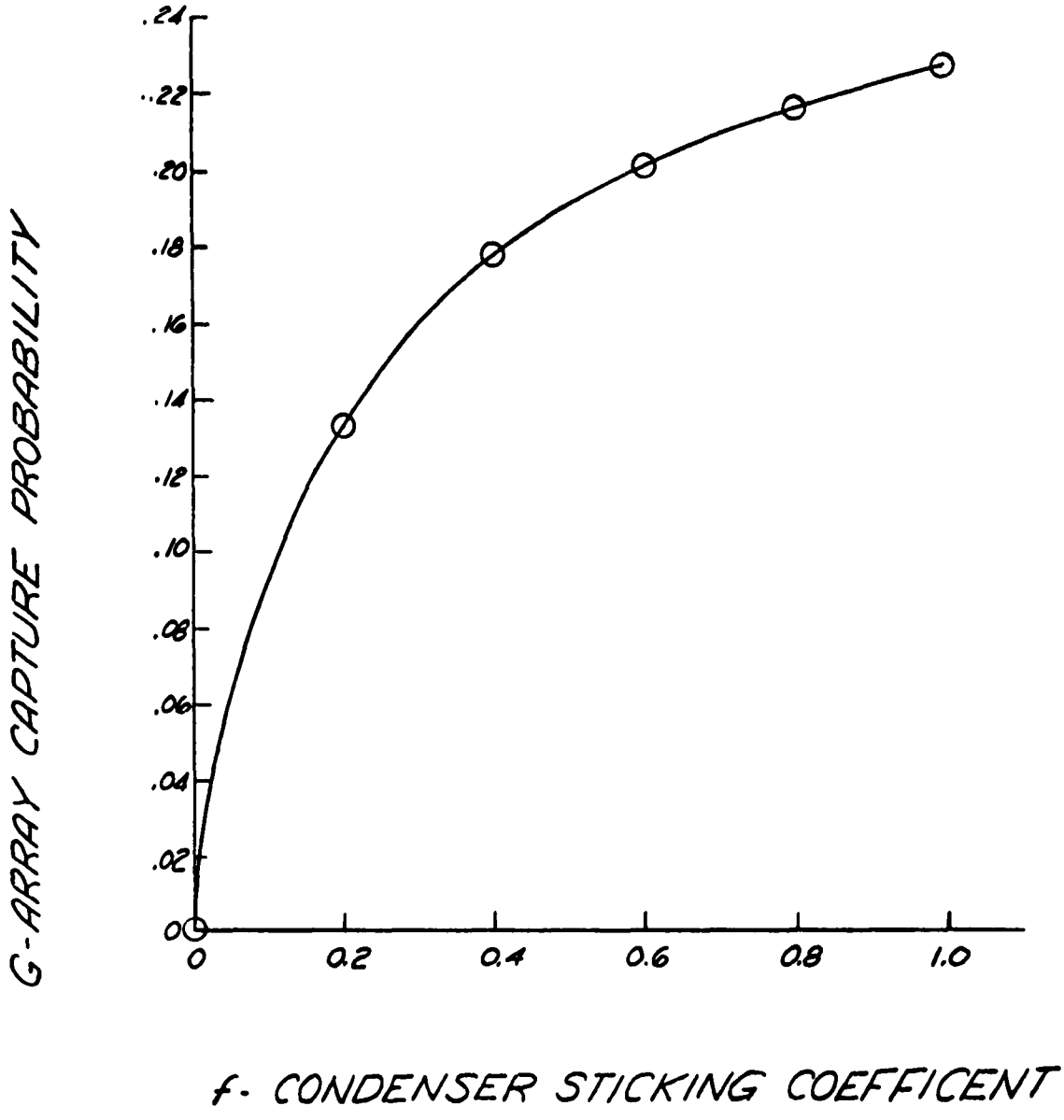

FIGURE 15

EFFECT OF CONDENSER STICKING COEFFICENT ON ARRAY CAPTURE PROBABILITY

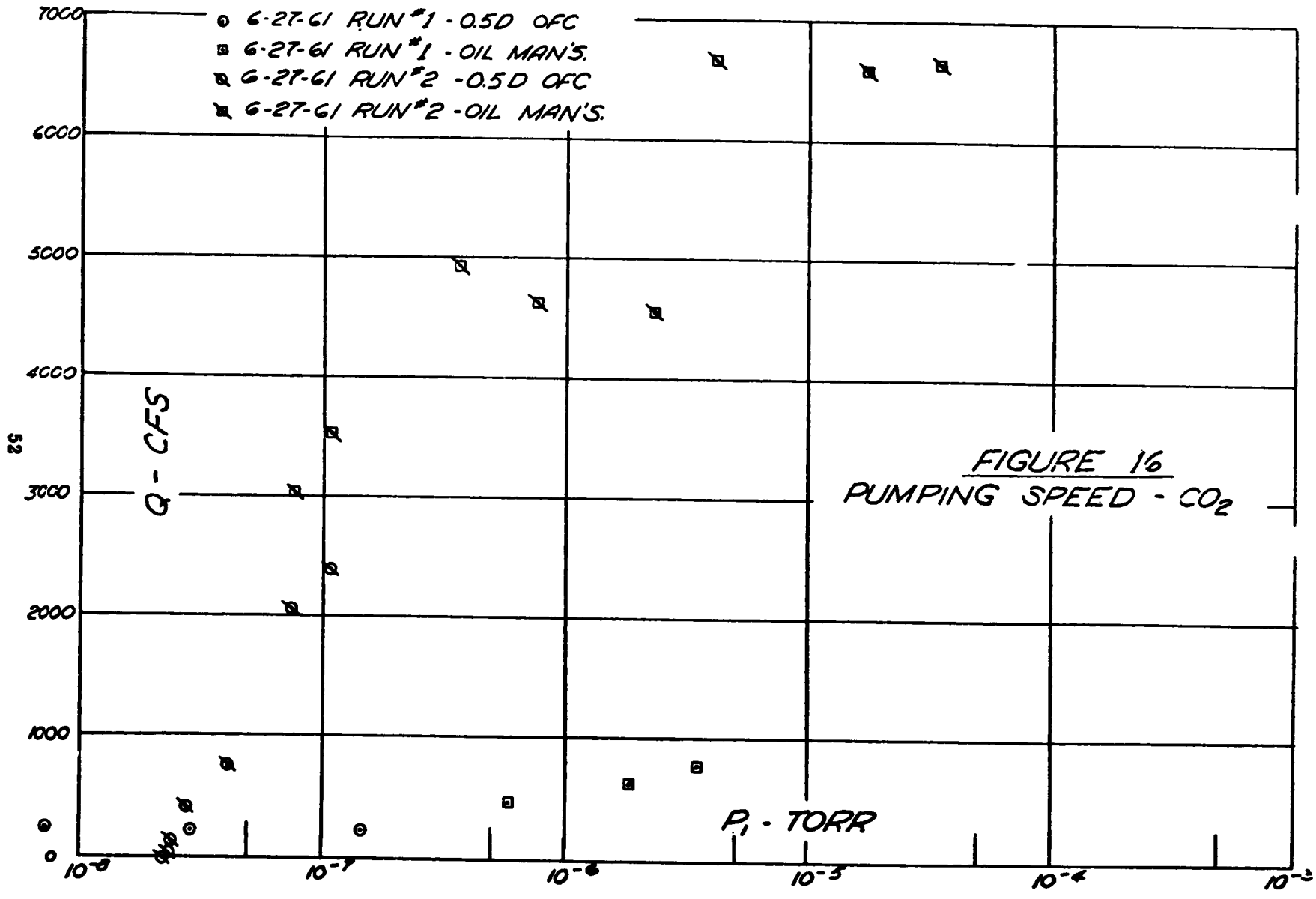

FIGURE 16
PUMPING SPEED - CO_2

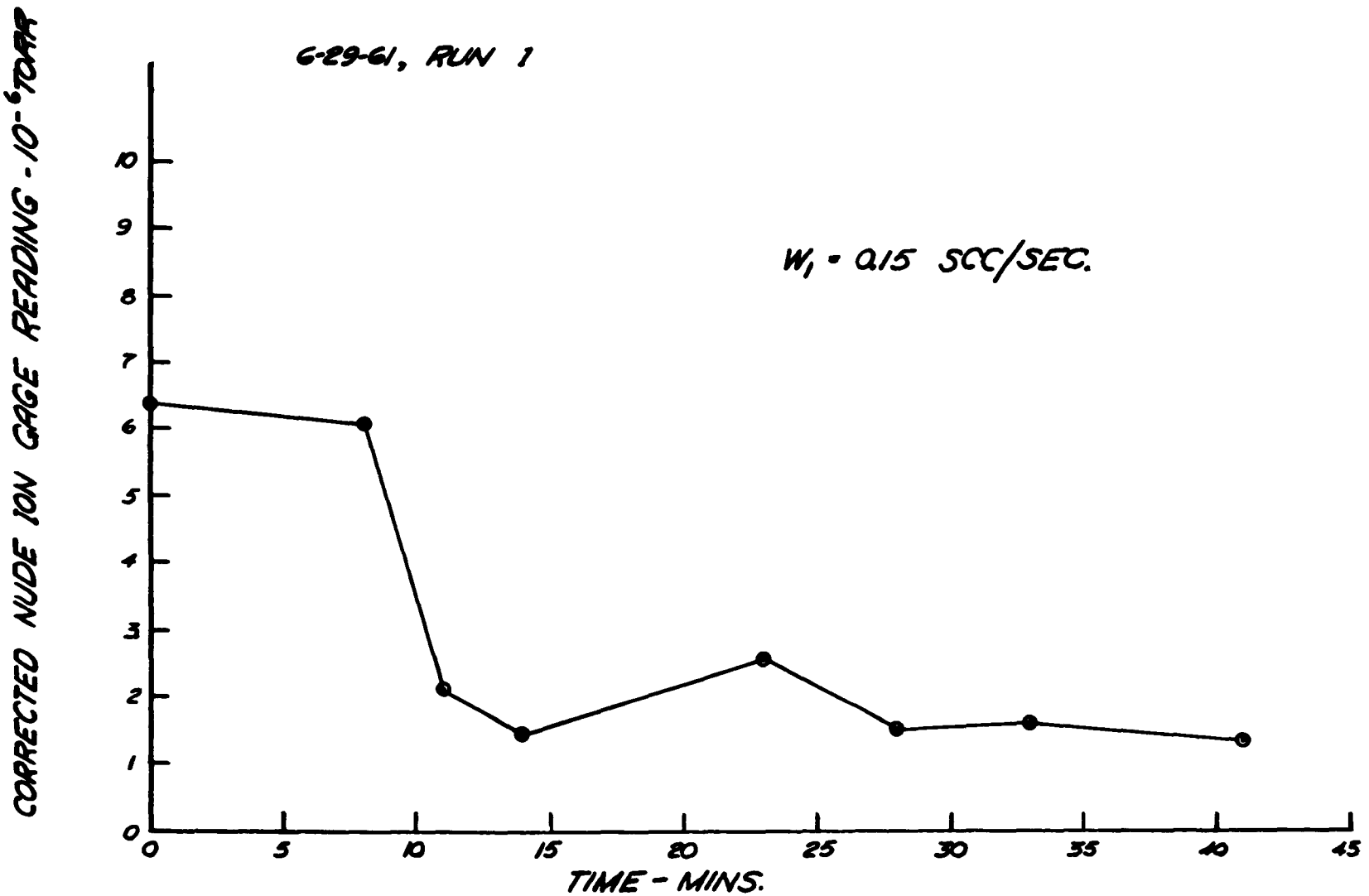

FIGURE 17. EFFECT OF CO_2 DEPOSIT THICKNESS ON UPSTREAM PRESSURE

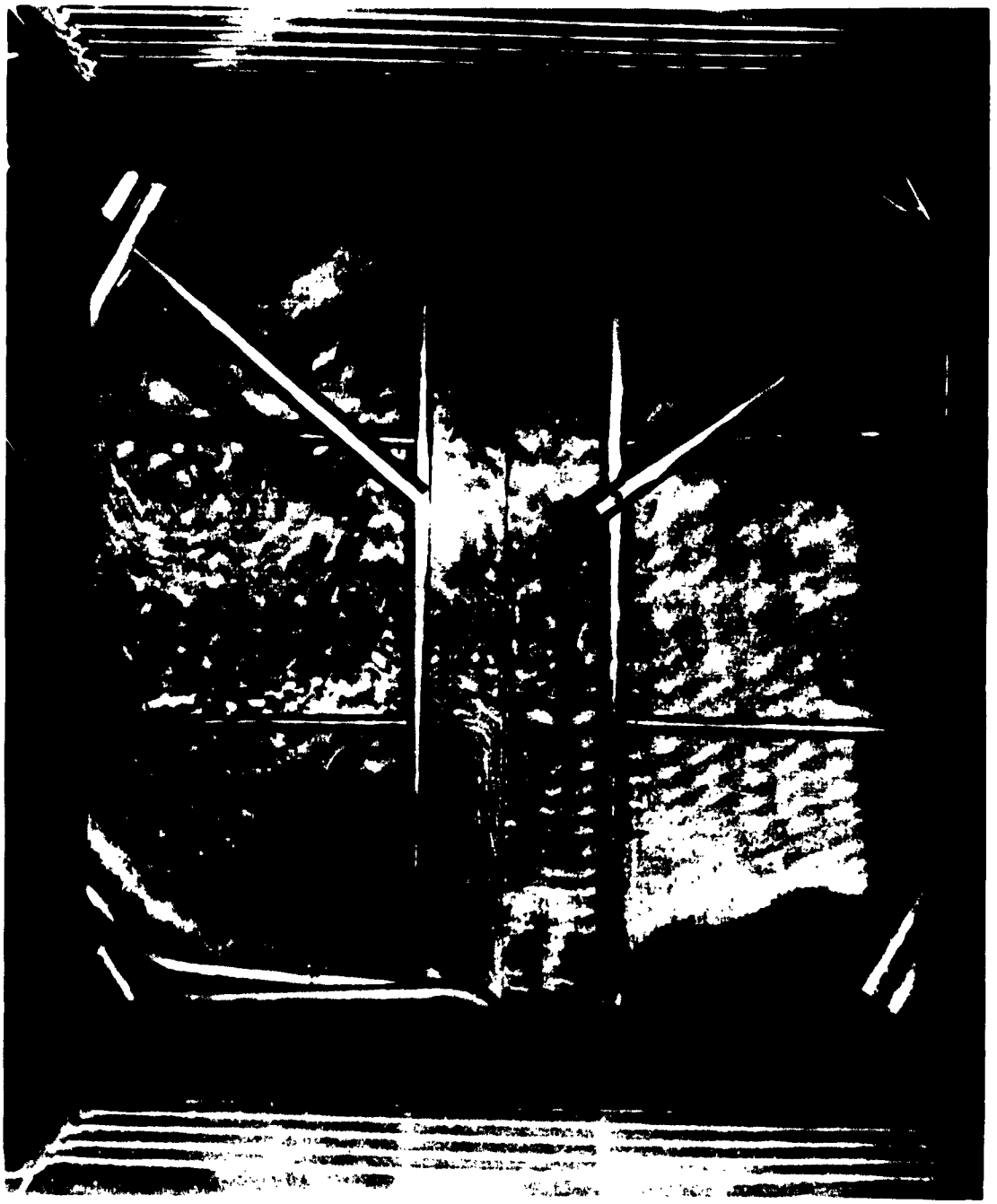

Figure 18 Directional Pressure Probes

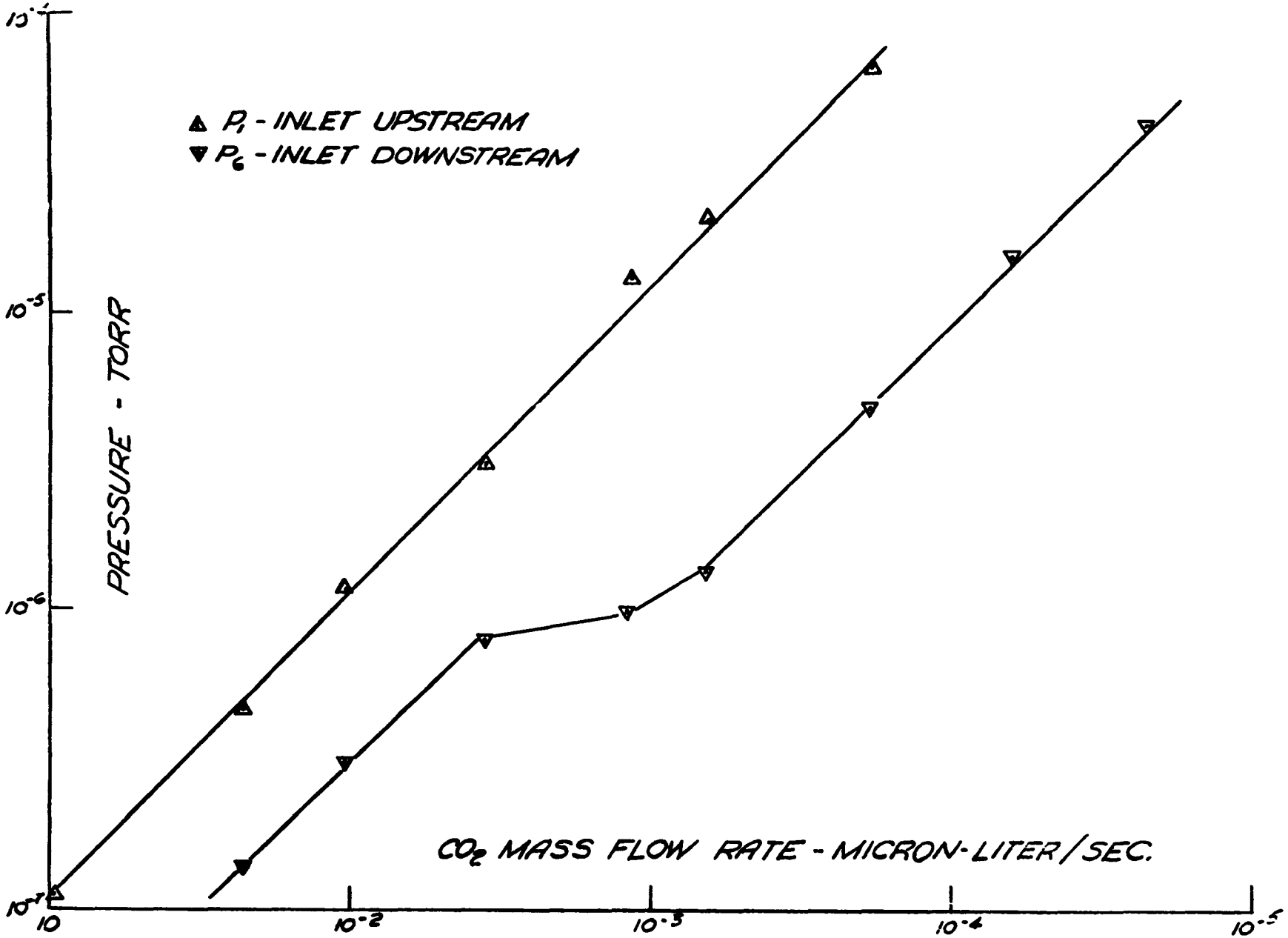

FIGURE 19. EFFECT OF GAGE INLET ORIENTATION ON PRESSURE MEASUREMENT

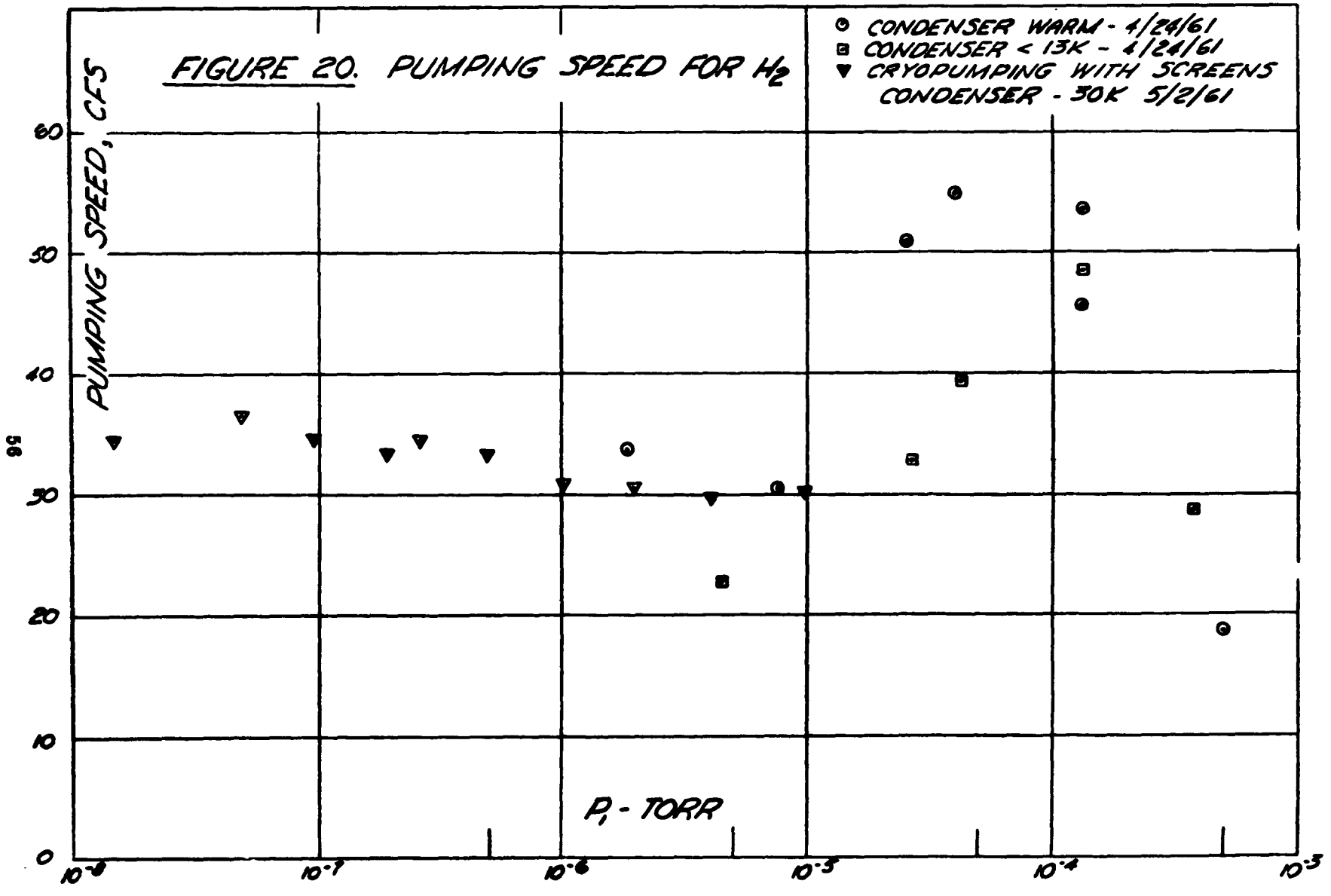
FIGURE 20. PUMPING SPEED FOR H_2
CONDENSER WARM - 4/24/61
CONDENSER < 13K - 4/24/61
CRYOPUMPING WITH SCREENS
CONDENSER - 30K 5/2/61
PUMPING SPEED, CFS
S
60
50
40
30
20
10
0
10^{-8}
10^{-7}
10^{-6}
10^{-5}
10^{-4}
10^{-3}
P_i - TORR

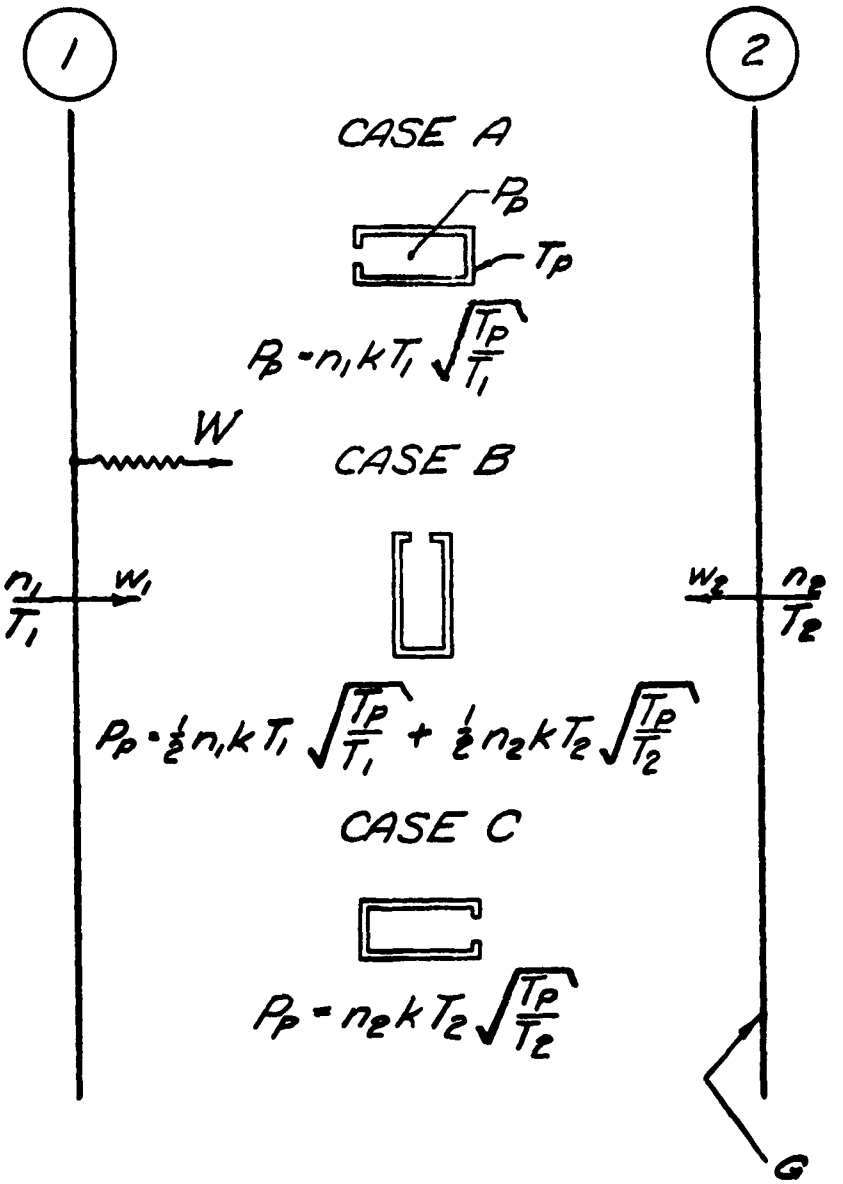

FIGURE 21
PRESSURES INSIDE AN OPEN-ENDED PROBE

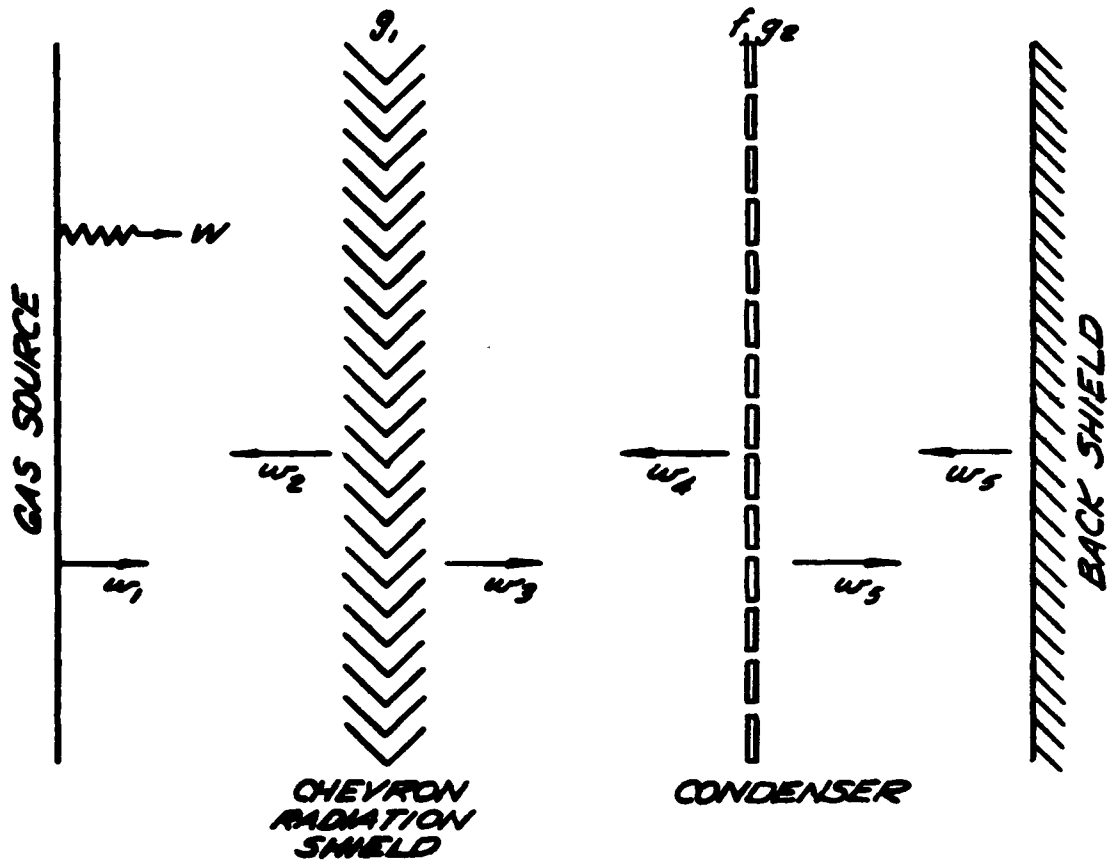

FIGURE 22 MODEL FOR ANALYSIS OF CHEVRON ARRAY

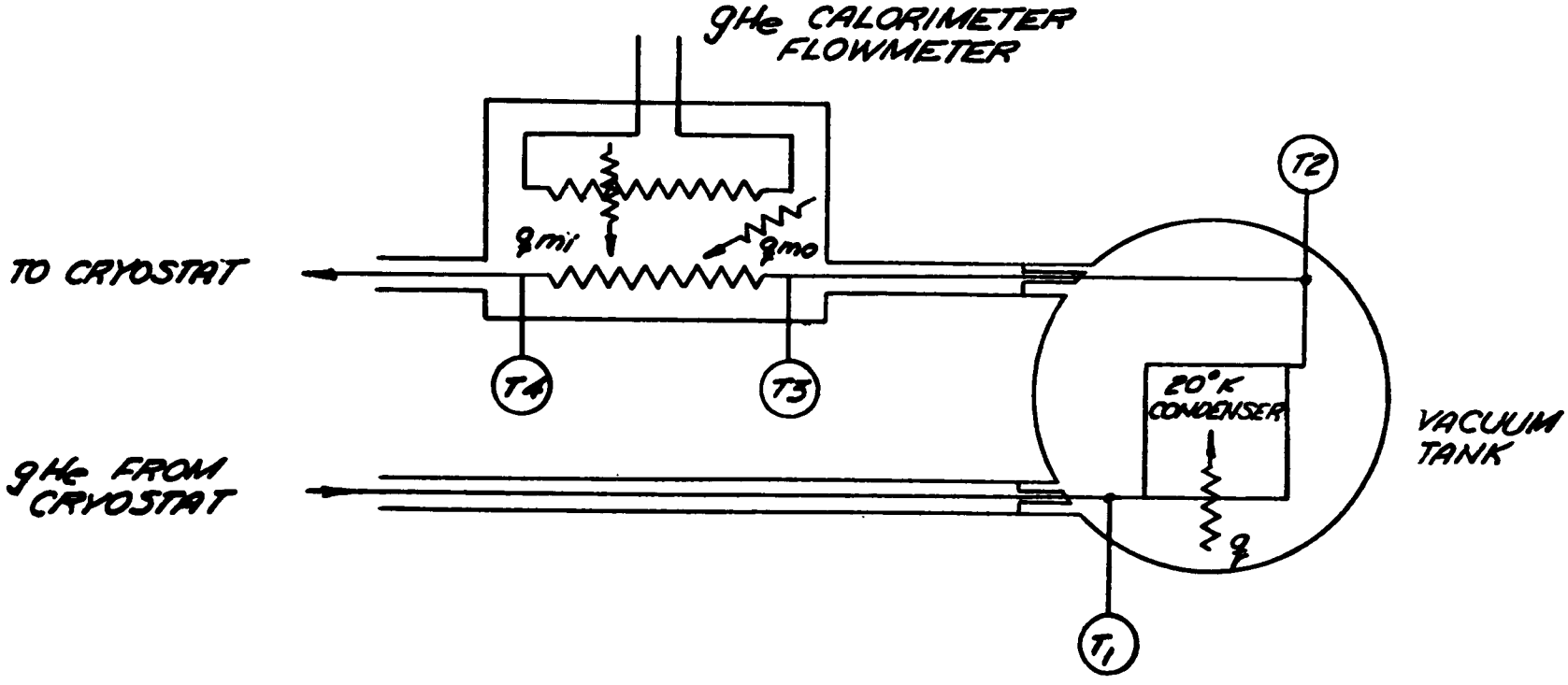

FIGURE 23
SCHEMATIC OF CONDENSER HEAT LOAD MEASUREMENT CIRCUIT

APPENDIX A - RELATIONS BETWEEN PRESSURE AND PUMPING SPEED DETERMINED BY AN OPEN-ENDED PROBE AND CAPTURE PROBABILITY

Consider a simple, open-ended probe placed between two infinite parallel planes, one a gas source (Plane No. 1) the other a gas sink (Plane No. 2), as pictured in Figure 21. Three different probe orientations are shown. The capture probability of the pumping surface (2) is G. The net mass flow rate from (1) to (2) is W. The absolute mass flow rates are w_1 from (1) to (2) and w_2 from (2) to (1). We will assume that there is no gas input at (2), i.e. the absolute evaporation rate from the sink is negligible. This condition will be met under most conditions, as discussed below. Then the flow rates are related by the following Equations:

$$1)\quad w_1 = \frac{W}{G}$$

$$2)\quad w_2 = W\left(\frac{1 - G}{G}\right)$$

In accordance with the procedure set forth in our feasibility study for Arnold Engineering Development Center[1], the absolute mass flows W_1 and W_2 can be considered as coming from equilibrium gas clouds at (1) and (2) with molecular densities n_1 and n_2 and temperatures T_1 and T_2. As a result we can write

$$3)\quad \frac{w_1}{A} = \frac{mn_1\bar{v}_1}{4}$$

$$4)\quad \frac{w_2}{A} = \frac{mn_2\bar{v}_2}{4}$$

where

$\bar{v}$ = mean molecular speed = $\sqrt{\frac{8\,kT}{\pi\,m}}$

m = mass of a molecule

k = Boltzmann's constant

Therefore, for P_p greater than about 10^{-9} torr, absolute evaporation may be neglected.

A definition of pumping speed based on the mass flow input, W, and the density upstream of the pumping surface apparent to a probe positioned as in Case B, will be useful in discussing experimental results. Thus

$$9) \quad \frac{Q_p}{A} = \frac{W}{A\, m\, n_p}$$

Because the gas inside the probe is assumed to be an equilibrium gas at temperatures T_p,

$$10) \quad n_p = \frac{P_p}{k\, T_p}$$

Combining (9) and (10) with Equation 6, we find that

$$11) \quad \frac{Q_p}{A} = \frac{2G}{2 - G} \cdot \sqrt{\frac{k\, T_p}{2\pi\, m}} = \frac{2G}{2 - G} \cdot \frac{\bar{v}_p}{4}$$

In using Equation 6 we imply that absolute evaporation from the condenser is negligible. Equation 11 above shows that when it is negligible, the pumping speed is independent of pressure.

The significant temperature turns out to be T_p, the probe temperature. In many conventional vacuum systems, the temperature of all components, including the pressure probe is uniform throughout and equal to the ambient level, and there is no question about what temperature is significant in an experimental determination of pumping speed. However, if the probe temperature differed from that of the rest of the system, it would have a direct effect on the experimentally determined pumping speed, as shown by (11). In systems employing cryogenic surfaces, the probe temperature may in practice differ from the ambient level, and its effect should be taken into account in interpreting experimental results.

APPENDIX B - RELATIONSHIP BETWEEN THE CHEVRON ARRAY CAPTURE PROBABILITY AND THE CONDENSER STICKING COEFFICIENT

Consider the simple model shown in Figure 22 where:

w = absolute mass flow

W = the net mass flow into the array

g_1 = the probability that a molecule will pass through the chevrons

g_2 = the probability that a molecule will pass through the condenser (equal to the percent open area)

f = the sticking coefficient on the condenser

The mass flow rates are related by the following equations:

1. $w_1 - w_2 = W$

2. $w_2 = (1 - g_1)\, w_1 + g_1\, w_4$

3. $w_3 = g_1\, w_1 + (1 - g_1)\, w_4$

4. $w_5 = g_2\, w_3 + (1 - g_2)(1 - f)\, w_5$

5. $w_4 = g_2\, w_5 + (1 - g_2)(1 - f)\, w_3$

The capture probability of the array as a whole, G, is given by

6) $$G = \frac{W}{w_1}$$

From the above,

7) $$G = g_1 \left\{ \frac{1 - 2(1 - g_2)(1 - f) + (1 - g_2)^2 (1 - f)^2 - g_2^2}{1 - (1 - g_2)(1 - f)(2 - g_1) + (1 - g_1)\left[(1 - g_2)^2 (1 - f)^2 - g_2^2\right]} \right\}$$

In our array, $g_1 = 0.23$[8] and $g_2 = 0.25$. The value for g_1 is for an aspect ratio (ratio of chevron length to spacing) of 6 which is appropriate to the

experimental array; hence it takes into account the effect of the end walls. Using these values of g_1 and g_2 we can calculate the effect of the sticking coefficient on, G, the over-all capture probability, from Equation 7. The results are shown in Figure 15, a plot of G versus f.

It is apparent from Figure 15 that the over-all capture probability is not extremely sensitive to the sticking coefficient provided that it is greater than about 0.5. This characteristic of a chevron-shielded condenser is due to the fact that once a molecule has penetrated the chevrons, the probability of its making more than one contact with the condenser (and therefore of its being captured) before traveling back out through the chevrons is rather high.

APPENDIX C - UNCERTAINTIES IN HEAT LOAD DETERMINATIONS

A schematic diagram of the condenser heat load measurement circuit is shown in Figure 23. The significant variables are defined below:

q = total heat load on the condenser; to be determined.

T_1 = condenser inlet temperature; indicated by a LH_2 vapor pressure thermometer.

T_2 = condenser outlet temperature; indicated by a LH_2 vapor pressure thermometer.

T_3 = flowmeter inlet temperature; indicated by a LH_2 vapor pressure thermometer.

T_4 = flowmeter outlet temperature; indicated by a LH_2 vapor pressure thermometer.

q_{mi} = heat input to flowmeter; measured by a wattmeter.

q_{mo} = background heat leak to flowmeter from radiation and conduction.

The condenser heat load is related to the measured variables by the relation

$$1)\quad q = \frac{T_2 - T_1}{T_4 - T_3} \cdot (q_{mi} + q_{mo})$$

q_{mo} was determined periodically by comparing the temperature rise across the flowmeter ($T_4 - T_3$) with a known input, q_{mi}, to that with $q_{mi} = 0$, while the gHe flow rate remained constant. Its value remains steady during a test at about 2 watts $\pm$ 0.1 watts.

The uncertainty interval in q, w_q, is related to the uncertainty intervals of the other variables by[12]

$$2)\quad \frac{w_q}{q} = \sqrt{\left(\frac{w_{T_1}}{T_2 - T_1}\right)^2 + \left(\frac{w_{T_2}}{T_2 - T_1}\right)^2 + \left(\frac{w_{T_4}}{T_4 - T_3}\right)^2 + \left(\frac{w_{T_4}}{T_4 - T_3}\right)^2 + \left(\frac{w_{q_{mi}}}{q_{mi} + q_{mo}}\right)^2 + \left(\frac{w_{q_{mo}}}{q_{mo} + q_{mi}}\right)^2}$$

Based on our experience, and typical operating conditions we estimate the following uncertainties in the variables on which q depends:

$$\frac{w_{T_1}}{T_2 - T_1} = \frac{w_{T_2}}{T_2 - T_1} = \frac{0.22^\circ K}{1.1^\circ K} = 0.2$$

$$\frac{w_{T_3}}{T_4 - T_3} = \frac{0.16^\circ K}{3.2^\circ K} = 0.05$$

$$\frac{w_{T_4}}{T_4 - T_3} = \frac{0.16^\circ K}{3.2^\circ K} = 0.05$$

$$\frac{w_{q_{mi}}}{q_{mi} + q_{mo}} = \frac{0.1}{5} = 0.02$$

$$\frac{w_{q_{mo}}}{q_{mi} + q_{mo}} = \frac{0.2}{5} = 0.04$$

From Equation 2 and the above conditions we find that

$$3) \quad \frac{w_q}{q} = 0.30$$

The condenser heat loads we have observed are between 1 and 2 watts. If we consider an average of about 1.5 watts, $w_q = 0.3 \times 1.5 = 0.45$ watts, or $\pm$ 0.23 watts. Thus, if a load of 1.5 watts were measured, the true load would be expected to lie between 1.27 and 1.73 watts. The uncertainty interval of 0.45 watts is largely due to the uncertainties in measuring T_1 and T_2 and should be fairly independent of the precise condenser heat load level in the range of interest.

To separate the influence of IR or solar irradiation, we must take differences in condenser heat loads measured at two different times, i.e., the heat load with irradiation, q_2, and the background load before irradiation is introduced, q_1. The difference, Δq, given by

$$4) \quad \Delta q = q_2 - q_1$$

is indicative of the effect of irradiation. The uncertainty in Δq, $w_{\Delta q}$, is given by

$$5) \quad w_{\Delta q} = \sqrt{(w_{c_1})^2 + (w_{q_2})^2}$$

The uncertainty in q_2, w_{q_2}, is 0.45 watts. The background, q_1, was not measured at the same instant as q_2, so in addition to the uncertainty in its measured value at the time the measurement was made we must also consider possible fluctuations of q_1 in time. Our experience indicates that such fluctuations are of the order of $\pm$ 0.1 watts.

Then

$$w_{q_1} \simeq \sqrt{(0.45)^2 + (0.2)^2} = 0.49 \text{ watts}$$

$$6) \quad w_{\Delta q} = \sqrt{(.49)^2 + (.45)^2} = 0.67 \text{ watts}$$

Thus, the uncertainty in the determination of Δq in Tests 2, 3, and 4 was approximately $\pm$ 0.34 watts.

The incremental heat load on the chevrons, associated with irradiation, ΔQ, is obtained from

$$7) \quad \Delta Q = Q_2 - Q_1$$

where Q_1 = background heat load on chevrons

Q_2 = heat load on chevrons with irradiation

The uncertainty in ΔQ, $w_{\Delta Q}$, is given by

$$8) \qquad \frac{w_{\Delta Q}}{\Delta Q} = \sqrt{\left(\frac{w_{Q_1}}{Q_1}\right)^2 + \left(\frac{w_{Q_2}}{Q_2}\right)^2}$$

The uncertainties in Q_1 and Q_2 are largely due to temporal fluctuations during measurement periods. Experience shows that

$$w_{Q_1} \simeq w_{Q_2} = 10 \text{ watts}$$

so that

$$\frac{w_{Q_1}}{Q_1} \simeq \frac{10}{55} = 0.182$$

$$\frac{w_{Q_2}}{Q_2} \simeq \frac{10}{115} = 0.087$$

and

$$9) \qquad \frac{w_{\Delta Q}}{\Delta Q} \simeq 0.20$$

In most of the tests, the uncertainty interval for condenser heat load measurements was greater than the observed increments in condenser heat load that coincided with the introduction of irradiation so that accurate estimates of the effect of irradiation are impossible. However, by combining the uncertainty intervals with the measured values we can place limits on what heat loads might be anticipated. The quantity of primary interest is the fraction of energy incident on the array which is transmitted to the 20°K condenser, q_T/q_i. For small q_T/q_i, the ratio is directly related to the experimentally determined quantities Δq and ΔQ by

$$10) \qquad \frac{q_T}{q_i} = \frac{\Delta q}{\Delta Q}$$

Therefore

$$11) \qquad {}^{(w)}q_T/q_i = {}^{(w)}\frac{\Delta q}{\Delta Q} = \frac{\Delta q}{\Delta Q}\sqrt{\left(\frac{{}^{w}\Delta q}{\Delta q}\right)^2 + \left(\frac{{}^{w}\Delta Q}{\Delta Q}\right)^2}$$

From the data in Table III and Equations 6 and 9, we see that

$$12) \qquad \left(\frac{{}^{w}\Delta Q}{\Delta Q}\right)^2 \ll \left(\frac{{}^{w}\Delta q}{\Delta q}\right)^2$$

so that

$$13) \qquad {}^{(w)}q_T/q_i \simeq \frac{{}^{W}\Delta q}{\Delta Q}$$

i.e., the uncertainty in the determination of Δq, the incremental heat load on the condenser, is controlling.

APPENDIX D

VACUUM INSTRUMENTATION ASSISTANCE BY NATIONAL RESEARCH CORPORATION

NRC Research Project No. 41-1-122

INSTRUMENTATION ASSISTANCE TO ARTHUR D. LITTLE, INC.

RE: CRYOPUMPING RESEARCH INVESTIGATION

Summary Report

July 14, 1961

John C. Simons, Jr.

Prepared under subcontract to

Arthur D. Little, Inc.
Acorn Park
Cambridge 40, Massachusetts
(GM20713)

for

Arnold Center
Contract No. AF40(600)899

by

Research Division
National Research Corporation
70 Memorial Drive
Cambridge 42, Massachusetts

TABLE OF CONTENTS

INSTRUMENTATION ASSISTANCE TO ARTHUR D. LITTLE, INC.
RE.: CRYOPUMPING RESEARCH INVESTIGATION
SPONSORED BY ARNOLD ENGINEERING DEVELOPMENT CENTER, USAF.

SUMMARY REPORT

1. INTRODUCTION

This is a summary report of assistance provided to Arthur D. Little, Inc. by National Research Corporation in the field of low density gas instrumentation and measurement. The purpose of this assignment is to provide a critical assessment of experimental determinations of pressure, pumping speed and gas composition, made by Arthur D. Little, Inc., in the course of a cryopumping research investigation sponsored by Arnold Engineering Development Center, U.S.A.F.

The scope of the services provided by National Research Corporation is briefly as follows:

1) Review the installation of ion gauges on the high vacuum cryopump test chamber at Arthur D. Little's Acorn Park site, provide a standard for calibration and assist ADL in calibrating the gauges under the condition of static vacuum in the chamber, and provide an assessment of the accuracy of pressure measurement under static vacuum conditions.

2) Review methods adopted by ADL for determining pumping speeds, observe measurements made during a typical test run, review the data and calculations for the run, and provide an assessment of the accuracy of the pumping speed determinations.

3) During the course of the above work, point out any aspects of the determinations of pressure or pumping speed which appear to be inadequate, and recommend improvements in technique which would yield results with greater accuracy or reliability, or would expedite execution of the test program.

4) Provide a summary report of the information provided Arthur D. Little during the program.

Note: An original requirement for assistance with gas composition measurements was subsequently withdrawn as later developments in the program made it unnecessary. The effort intended for this work was devoted to additional gauge and pumping speed calibration.

Two interim memoranda, covering gauge calibration and pumping speed measurements respectively, have previously been submitted to Arthur D. Little (Ref. 1 and 2). It is understood that copies of these memoranda have been appended to ADL'S progress report to Arnold Center for the period ending May 15, 1961. This summary report is intended to be complete in itself, so that reference to the earlier memoranda is unnecessary, except for detailed data which are not regarded as of general interest.

2. GAUGES AND PRESSURE MEASUREMENTS

2.1 Installation of Ionization Gauges

Six hot-cathode ionization gauges are installed at various places on the cryopumping test facility. These six gauge locations are designated by P numbers and are identified as follows:

Gauges P1 and P6	are ultrahigh vacuum gauges of the Bayard-Alpert type and are mounted on the main chamber several inches upstream of the face of the cryopumping array.
Gauge P5	is a similar type and is mounted at the rear of the main chamber, near the diffusion pump duct.
Gauges P3 and P4	are conventional ionization gauges and are mounted on the right and left inlet plenum chambers respectively.
Gauge P12	is an ultrahigh vacuum gauge of the Bayard-Alpert design, but differs from the above gauges in that it is of the exposed or so-called nude configuration, rather than mounted

Gauge P12 cont.	in the conventional glass envelope. This gauge is also mounted on the main chamber, and was installed midway through the experimental program.

The installation of all gauges appears satisfactory for the experiments undertaken.

For various reasons a number of gauge failures were experienced during the program. These gauges were replaced, necessitating additional calibration beyond the initial effort.

At pressures above 10^{-4} torr (and in some instances at pressures as low as 10^{-5} torr), thermionic vacuum gauges are subject to a number of errors when operated at the electron emission current recommended by the manufacturers. Principal sources of these errors are ionic space charge near the collector, changes in the electron path length at higher pressures, multiple ionization, and recombination (see references 3 and 4). The effect of these errors has only recently achieved some degree of general recognition. Their importance lies in the fact that ion gauges are customarily calibrated (if at all) by comparison with a mercury McLeod gauge over just the pressure range where these errors predominate. The gauge factor used at lower pressures, where the ion gauge is ordinarily quite linear, may therefore be poorly chosen because of systematic errors over the calibration pressure range of which the experimenter is unaware.

To minimize the non-linearity at higher pressures, Nottingham (Ref. 4) has urged that thermionic vacuum gauges should be operated with electron currents of a few microamperes, some three orders of magnitude smaller than manufacturer's recommendations. Commercially available control units cannot function in this manner. In order to convert the three different gauge control units to this method of operation, NRC personnel designed suitable circuit modifications and provided Arthur D. Little, Inc. with sketches and instructions for making the conversion. Satisfactory operation of the units was verified after ADL personnel had made the changes recommended.

Operation with emission currents in the microampere range was recommended for gauges P1. P5 and P6 at all pressures above 10^{-5} torr and for gauges P3 and P4 at pressures above 10^{-4} torr. At lower pressures, emission currents 1000 times higher were recommended. The control circuit for gauge P12, which was added later, was not converted and this gauge was always operated in the milliampere emission range. This gauge, which must still be regarded as somewhat in the experimental stage, was added(by ADL personnel)with the hope that it would produce more stable and reliable information than the gauges already in use. This level of confidence in its indications was not achieved, but the gauge proved useful in interpreting other gauge readings, especially during calibration.

2.2 Standard for Gauge Calibration

As a standard against which to calibrate the thermionic vacuum gauges, NRC provided a mercury McLeod gauge and adapted it to the cryopump facility at Acorn Park. This particular gauge was selected because the bore diameter of the capillary had already been carefully measured in our laboratories and was accurately known.

The effective height of the closed capillary was then determined (three separate determinations) by Clark's method (Ref. 5). The resulting value is estimated to have a systematic uncertainty (95% confidencelevel) of $\pm$ 0.32 mm.

A random uncertainty is introduced in measuring the height of the mercury column in the capillary. In a set of 12 measurements, the standard deviation in determining the height of a single mercury column was found to be 0.05 mm. For accurate measurements, column heights should be measured with a cathetometer capable of reading at least to 0.1 mm. The overallrelative probable error, accounting for both zero uncertainty and reading errors, is given by:

$$\frac{\delta p}{p} = \frac{1.03 \times 10^{-3}}{\sqrt{p\ [\text{torr}]}} \qquad (1)$$

and is seen to be a function of the pressure being measured. Figure A-1 shows this graphically and may be used as an estimate of the relative uncertainty (95% confidence level*) of the individual McLeod gauge measurements made during the calibration procedure.

Capillary forces at the mercury interface are another source of error. The action of capillary forces tending to depress the height of a mercury column in small bore tubing is well known. These forces become increasingly important in smaller diameter tubing; their magnitude may vary considerably depending on the condition of the mercury and the surface cleanliness of the glass wall. Variability in mercury column heights can be found during an individual measurement, depending on whether the gauge is tapped or not, the time interval between compression and column reading, and related factors (Ref. 7). Experience indicates that a moderate amount of tapping a moment or two before reading the gauge helps to give repeatable results; this procedure has been found helpful here. Tapping will of course give no improvement in systematic errors.

In an effort to balance out the effects of systematic capillary forces, the open and closed capillaries of a McLeod gauge are ordinarily made from tubing with exactly the same bore. In any particular case, however, differences in surface conditions within the two capillaries may result in unequal capillary forces which will be reflected in an erroneous differential column height as a measure of the pressure of the gas confined in the closed capillary (Ref. 7 and 8). At pressures above 10^{-4} torr and in capillaries as large as in the present gauge (1.5) the capillary depression difference is generally negligible, and during the initial calibration phase this was found to be the case. During a later calibration of replacement gauges, inconsistent data obtained led to a re-examination of this problem. It was found that on that particular day an

*Note: Since estimates of probable error involve statistical measures computed from finite samples. and are therefore subject to sampling fluctuations, they need to be qualified by a "confidence level" or objective probability that the error in any one measurement result will not exceed the limits stated (see Ref. 6).

appreciable capillary depression difference did exist and was in one instance as high as 2 mm. Such variations are usually attributable to contamination of the capillary surfaces which is likely in this case because the gauge had been reconnected to the system after standing idle (exposed to the atmosphere) for several weeks. This explanation tends to be confirmed by a recheck a few days later which showed that the capillary depression differences were again negligible. The contamination was evidently pumped away by the vacuum system during the intervening few days. Where a significant capillary depression difference exists, its extent should be determined and suitable corrections made. This was done for the particular data concerned. Some uncertainty is attached to other data taken a few days earlier, because this effect was at that time not appreciated by ADL personnel and its extent was not measured. It is not unreasonable to presume that the capillary depression was the same as or greater than that measured a few days later.

When the capillary depression correction is appreciable, then the uncertainty in its magnitude is also likely to be significant. Taking 0.2 mm as a reasonable estimate of this uncertainty, expression (1) for the combined relative probable error is replaced by

$$\frac{\delta p}{p} = \frac{1.47 \times 10^{-3}}{\sqrt{p}} \qquad (2)$$

with a 95% confidence level. This revised error estimate is also shown in Figure A-1.

At lower pressures additional sources of error in McLeod gauges become significant. An important source is distortion of the closed capillary in the vicinity of the closure seal, which results both in non-uniform cross-section of the bore and in optical errors in measuring the meniscus height. It is generally unwise to rely on the McLeod gauge measurements below 10^{-4} torr unless the instrument is specifically designed for the purpose and is carefully rechecked daily. In Figure A-1 the error estimates are deliberately not projected below about 10^{-4} torr because of (1) the difficulty in estimating the additional errors, and (2) the limited usefulness of a reference whose overall uncertainty exceeds $\pm$ 15%.

A cold trap and valve are installed in the line connecting the McLeod gauge to the vacuum chamber. It is important that the trap be kept filled with liquid nitrogen whenever the valve is opened, and it is understood that this practice has been followed.

When a McLeod gauge is first attached to a vacuum system, its walls will outgas for some time. If of sufficient magnitude, this outgassing may result in errors and may be readily checked by closing the valve to the vacuum chamber and determining the rate at which the indicated pressure rises. This check has been made whenever the McLeod gauge was installed or reinstalled on the chamber and no significant outgassing has been found.

Because of the tubulation connecting the McLeod gauge to the chamber, the pressure of the McLeod gauge itself will lag behind rapid changes of pressure in the chamber. Whenever the chamber pressure has changed by more than a factor of 3 or so, it is advisable to wait several minutes until the gauge reaches equilibrium with the newly established chamber pressure. The reliability of the McLeod gauge reading can be checked by taking a second reading to see if there has been any change. This viewpoint is familiar to ADL operating personnel.

2.3 Calibration of Ionization Gauges

The initial five thermionic gauges were calibrated statically against the McLeod gauge by evacuating the chamber to the lowest pressure attainable with the two-inch diffusion pump and then back-filling the chamber to various static pressures with a known gas. With both the diffusion pump port and gas inlet valve closed, the pressure of the trapped gas was observed simultaneously by the McLeod gauge and as many as three of the ion gauges. Nitrogen, hydrogen, and helium were used as known atmospheres.

On several occasions it became necessary to replace ion gauges that had been accidentally damaged or failed for other causes. Static calibration against the McLeod of all ion gauges was therefore carried out on two later occasions. As an interim procedure, newly installed gauges were calibrated by comparison with the other gauges on the system whose calibration was already well known.

In any calibration procedure, the objective is to provide a knowledge of the response of the instrument over its entire range of operation. Thermionic vacuum gauges are generally regarded as linear devices at pressures below 10^{-5} torr, down to the point where the X-ray effect becomes significant. At pressures above 10^{-5} torr, deviations from linearity exist and should be determined for each gauge type since they are dependent upon geometry and operating conditions. Even at emission currents of a few micro-amperes, these non-linearities exist and should be determined if accurate results are required. The advantage in using low emission current is that the non-linearities are greatly reduced from those existing at higher emission currents, even though not eliminated completely.

Thermionic gauge calibration has two objectives: First, to provide the necessary gauge factor to be used at pressures below 10^{-5} torr (under the assumption that the gauge is linear in this region), and second, to determine the specific deviations from linearity at pressures above 10^{-5} torr. This information can be derived from the experimental data most easily by plotting the logarithm of the ratio of ion gauge to McLeod readings as dependent variable, with respect to the McLeod indication (assumed to be the "true" pressure) as independent variable. Figure C-1 is representative of the relevant information plotted in this way. Also shown are the estimates of uncertainty attached to each point; the basis of these estimates will be discussed later. At low pressures, the ultimate or background pressure in the chamber is an appreciable part of the pressure being measured by the ion gauge. This background pressure must be predominately due to water vapor since it is not measurable with the trapped McLeod gauge. To minimize the distortion in the results from this effect a background pressure was subtracted from each ion gauge reading, and the uncertainty estimates include a contribution for the uncertainty with which the background pressure is known.

The reason for plotting the data in this way is that a horizontal line would result if the device were linear. At low pressures it must be assumed that the curve becomes horizontal. A "best-fit" curve has therefore been drawn through the data points with the additional restriction that it must asymptotically approach the

horizontal at pressures below 10^{-5} torr, while at higher pressures it should have the general form already established as characteristic of such gauges (see reference 4). The figures noted at the left of the curves in Figure C-1 are the asymptotic fractions of the true pressure which are indicated by the gauge for the three gases, nitrogen, hydrogen and helium.

This procedure was followed by NRC personnel in the reduction of the first set of calibration data, and was adopted by ADL personnel in subsequent data reduction.

The later calibration data taken included also an intercomparison of ion gauges at reduced pressures, in the range where all of these gauges should be substantially linear. The resulting data appeared to have a number of inconsistencies, but a closer analysis indicated that the differences were substantially within the limits of uncertainty to be expected with such gauges. Since it is the purpose of this program to provide the best possible experimental information on cryopumping, these later calibration data were re-evaluated and a "best-fit" estimated to be most consistent with all of the available data was chosen.

2.4 Assessment of Accuracy of Pressure Measurements

Overall accuracy of any measurement is influenced by a number of factors including inherent instrument accuracy, calibration procedure, operating procedure, and application. The accuracy of ion gauge readings is influenced by meter accuracies, ability to read the meter ability to zero the amplifier, and ability to set the electron current at a specified value. These may be regarded primarily as random errors. Values of these errors have been estimated and are included in the uncertainties shown in Figure C-1. Systematic errors in the instrument will tend to be placed in evidence during calibration.

The McLeod gauge used as a standard is also subject to errors which have been discussed previously.

A detailed consideration of all possible uncertainties in the gauge calibration has been made but is too extensive to be presented here. From this analysis, however, a set of recommended calibration curves was prepared for the first five gauges calibrated. A representative curve is given in Figure D-2. The information is presented

in a form of correction factors, by which each gauge reading should be multiplied to give the best estimate of true pressure.

Operating procedure is important to achieving accurate pressure measurements. Gas evolution from contaminated surfaces (both gauge elements and walls of the glass envelope) and pumping by overly clean surfaces can introduce appreciable errors in ion gauge measurements. The optimum procedure is therefore one which achieves an equilibrium between the gas in the gauge and that adsorbed on the surfaces, so that there is no net flow of gas to or from the surfaces. Outgassing rates are relatively slow and therefore equilibrium is achieved most quickly by starting with a surface that has too little gas rather than one with too much: The procedure recommended is:

1) "Outgas" (degas) the gauge following manufacturer's recommendations.
2) Operate the gauge normally for at least ten minutes before taking measurements, using the electron currents specified in Memorandum 1.
3) Do not switch back and forth from one electron current to another unnecessarily as it is important to establish temperature equilibrium of the gauge envelope.
4) Sorption of gas on the gauge surfaces is most significant at low pressures and therefore, other things being equal, it is preferable to plan experiments that start at low pressures and progress to higher pressures.
5) High temperature degassing of the gauge gradually deposits a tungsten film on the inside of the gauge envelope. The leakage resistance between filament and grid will eventually become low enough that the leakage current is a sizable fraction of the emission current, when operated in the microampere range. Gauge accuracy is then seriously degraded; consequently, excessive and unnecessary degassing is as much to be avoided as insufficient degassing.

Using proper corrections derived from the calibration data, the overall uncertainty of individual static pressure measurements with ion gauges P1, P3, P4, P5 and P6 is estimated to be $\pm$ 40% (95% confidence level). These uncertainty estimates assume care in the taking of measurements, with attention to zero settings, amplifier balance, meter reading, and particularly to degassing which must be sufficient but not excessive. Careless operation, particularly with regard to degassing, can produce readings in error by as much as a factor of five. In most instances operational errors exceed those inherent in the instrument, but need not with suitable care.

The uncertainties estimated for pressure measurements arise from several different sources of error. Some of these are systematic errors, occurring consistently in each measurement. Others are completely random errors (such as uncertainty in reading a meter) and contribute "scatter" because the error in an individual measurement is entirely independent of that in other measurements. A third class of errors which can be quite misleading in the interpretation of data comprises those characterized by slow drifts (over periods of an hour or more), generally accompanied by discontinuities at intervals when a balance adjustment is reset (for example, periodic resetting of the amplifier null point). Errors of this third class are random over periods of days and weeks, but from a short term perspective (such as for a consecutive set of measurements during a single run) must be regarded as systematic. The internal consistency (relatively high precision) of a set of readings taken in a single run can easily suggest a higher level of accuracy than the results in fact deserve. This possibility of misinterpretation requires extra care in reviewing the results.

Some experiments have been made using carbon dioxide as the working gas. Calibration of ion gauges against a McLeod gauge is quite difficult with CO_2 because of the relative ease of condensation. Other investigators (see reference 9) have made careful measurements with CO_2. For these reasons, direct calibration with CO_2 was decided against. Instead it was recommended that CO_2 measurements be treated by first calculating the equivalent nitrogen pressure, and then multiplying the value obtained by 0.69. The uncertainty in this factor can be taken as $\pm$ 10% (95% confidence level).

Water vapor, besides entering strongly into sorption reactions, attacks the hot tungsten filament of an ion gauge, more or less rapidly changing its calibration and eventually resulting in failure. Experiments with water vapor have been strongly advised against until all other relevant data with less active gases have been obtained.

3. PUMPING SPEED DETERMINATIONS

3.1 Methods of Determining Pumping Speeds

Three different methods for determining pumping speed have been used by Arthur D. Little, Inc., in this program. Each of these involves the measurement of mass flow rate and of pressure at the cross-section where pumping speed is desired. In each case pressure at the cross section is measured in the same way (by an ion gauge) and so we are really considering three different methods for determining mass flow rate.

For measurements of mass flow rate at relatively high chamber pressures, where mass flow rates are sufficiently high, rotameter devices were used, operated at substantially atmospheric pressure. At lower chamber pressures, the known conductance of an orifice was used, together with measurement of the upstream pressure. For calibration purposes, an oil manometer was provided (on loan) by National Research Corporation; later this instrument was also used during actual research experiments.

Rotameter devices, when properly installed, perform well within the range for which they are intended. For very accurate work, it is advantageous to use individual calibration curves for each gauge.

Where molecular flow conditions exist, the orifice is inherently a very accurate means of measuring mass flow rates. When properly used, the limiting error is the accuracy with which the upstream pressure can be measured. Pressure measurements made with a calibrated ion gauge can therefore lead to mass flow rate measurements with an uncertainty for individual determinations of the order of $\pm$ 40% (95% confidence level). To achieve this accuracy, considerable care is necessary both in installation and operation; the conditions that should be met have been discussed in Memorandum No. 1 (Ref.1). These conditions are well understood by ADL personnel who made several modifications in an effort to provide the most accurate orifice metering arrangement possible. Initial calibration tests of the orifice arrangement were made by NRC personnel using an oil

manometer and indicated the need for changes which were subsequently made. After the changes, additional calibration checks were made by ADL using the oil manometer. These last calibration results were evaluated by ADL.

3.2 Oil Manometer Measurements of Pumping Speed

To provide a check on measurements of pumping speed made during a typical test run, an oil manometer was connected to the system. The oil manometer is a device for admitting a known quantity of gas into the system, at substantially a uniform rate that is determined by the characteristics of the system. The time interval during which the known quantity of gas is admitted is measured with a stop-watch. The principle of operation is described by Dushman (Ref. 10). Sources of error have been discussed in Memorandum No. 2 (Ref. 2); by proper design and operation the total error can be reduced to within a few percent.

The first speed calibration measurements were made while the system was pumping dry nitrogen, condensing on surfaces cooled to approximately 20° K by circulating helium. Fourteen measurements were made with the oil manometer, with chamber pressures ranging from 8×10^{-7} to 6×10^{-4} torr, and flow rates from 7 to 9500 micron -liters per second at room temperature. Chamber pressures were measured by ion gauges P1 and P6, mounted on the side walls of the chamber about six inches upstream from the front face of the cryo-baffle configuration. Pumping speed is always defined in terms of a specified reference plane across which the gas flows, and it must be remembered that the necessary pressure measurements of the gas are to be made at the reference plane. Locating the gauges so as to provide representative reference plane measurements is always a problem, and in this instance the gauges are placed as well as is possible.

In reducing the data, the ion gauge readings were corrected according to the curves given in Memorandum No. 1 (Ref. 1), and the oil manometer constants were adjusted for additional volume introduced by extra tubing used to connect the manometer to the throttling

valve at the inlet to the cryo-chamber. From this data the pumping speed at the reference plane is easily computed.

While the manometer measurements were being made, pressure in the plenum chamber through which the nitrogen was admitted was measured by ion gauge P4. With this additional information, the effective conductance of the orifice may be computed. This particular set of data led to mass flow rates which, calculated from the theoretical orifice conductance, were about 70% of those calculated from the oil manometer data. This indicated difficulty with the orifice arrangement (very likely leakage past the orifice plate), and corrective measures were taken. Having no permanent value, the data from these experiments are not included in this report but may be found in Memorandum No. 2 (Ref. 2).

Although the oil manometer was originally intended as a reference standard for calibration, arrangements were made to use it for mass flow rate measurements during most of the subsequent experiments because of the improved accuracy it offers. As an added precaution, the parameters of the manometer were remeasured and the gauge constants recalculated. The new values agreed within 3% of those previously used.

3.3 Errors in Pumping Speed Measurements

In the determination of pumping speed, two quantities must be measured: Mass flow rate,and pressure at the reference plane.

Orifice mass flow rate measurements are subject to two classes of error. The first class comprises those errors due to baffling and plenum chamber configuration, which influence the effective conductance and are largely systematic. Included also in this class are errors due to the location of the gauge so that it is providing a false indication of the mean pressure within the plenum chamber volume. For accurate measurements it is desirable to measure experimentally the effective conductance, and if this differs significantly from the calculated value to modify the orifice configuration. For an orifice of finite thickness, reconductance calculated from kinetic theory for an infinitely thin plate should be reduced

following Clausing (Ref. 11). If the mean-free path in the gas upstream of the orifice is less than 3 times the orifice diameter, the correction suggested by Liepman (Ref. 12) should be considered. If the experimental and theoretical values cannot be brought into agreement, then the experimental value should be used.

The second class of errors in orifice flow rate measurements comprises those associated with ion gauges. The mass flow rate is calculated as the product of the upstream pressure (as measured with an ion gauge) and the previously determined conductance of the orifice. The errors inherent in ion gauge measurements (discussed in Memorandum No. 1, Ref. 1) are likely to predominate in an optimum situation where all errors have been minimized insofar as is possible. Ion gauge errors are largely random, provided the gauge has been carefully calibrated.

Using an oil manometer, the uncertainty in determining the effective conductance of the orifice should be of the order of $\pm$ 40% (95% confidence level) for an individual measurement. The uncertainty is reduced by a factor of approximately $1/\sqrt{n}$ if one takes the mean of n completely independent measurements. If sufficient measurements are taken (over a long enough time to average out the random error in ion gauge readings), the uncertainty in the conductance value can probably be reduced to about $\pm$ 20% (95% confidence level). Because of the uncertainty, the value assumed for the effective conductance will probably differ from the "true" (but unknown) value and therefore introduces a bias error in the subsequent flow rate determinations. The comparison of several measurements relative to each other will be more precise than accurate since they are affected equally by this bias error. The random uncertainty or scatter introduced in orifice measurements by the pressure measurements of gauges P3 and P4 has previously been estimated to be $\pm$ 40% (95% confidence level) for individual measurements.

Direct calibration of the rotameters used at higher flow rates was not made since the oil manometer is not well suited to such a comparison. On the other hand, manufacturer's estimates of the

errors in these devices are regarded as reliable, and generally insignificant compared to errors from other sources.

Measurements with the oil manometer have previously been estimated to be accurate within a few percent, which is again an insignificant error compared to errors from other sources.

In addition to mass flow rate errors just discussed, measurements of pumping speed are subject to errors in ion gauge measurements at the reference plane. The uncertainty of individual ion gauge measurements, including reading errors, has previously been estimated as $\pm$ 40% (95% confidence level) provided that proper operating procedures are adhered to, with particular attention to degassing practice. Since ion gauge errors are largely random, improvement in accuracy can be obtained by taking a large number of measurements, provided that these measurements are taken over a considerable period of time in order that the slowly changing random components are averaged out.

When orifice measurements of mass flow rate are used, the pumping speed determination is subject to the independent uncertainties of two ion gauges. In this situation some improvement in overall accuracy is possible by direct static comparison of the ion gauges with each other, over a pressure range where they can both be considered linear. The range 10^{-6} to 10^{-5} torr is suitable, and is noted to be lower than pressures attainable with a McLeod gauge. This procedure may not provide particularly good absolute accuracy for the individual gauges. This is irrelevant, however, because the pumping speed calculation involves only the ratio of the two ion gauge readings. The effect of systematic ion gauge errors is therefore largely eliminated. Careful attention to minimizing random errors is still required. This procedure has been used by ADL in some experiments.

An additional error may arise from non-random molecular flow patterns within the main chamber, so that the pressure "seen" by

the ion gauge may not be representative of the mean "pressure"* at the reference plane. Such effects are of course minimized insofar as possible by suitable design. The principal factor causing non-randomness in the flow patterns is pumping by the cryo-array. If the pumping speed for nitrogen is about 250 cu ft per second, then it can easily be calculated that the average residence time of a nitrogen molecule in the chamber is the order of 60 milliseconds and on the average it makes about 20 collisions with the walls before being pumped away. Under these conditions, the pressure gauge indication can be expected to be a reasonably reliable measure of the pressure within the chamber, within probably $\pm$ 10%.

On the other hand, a similar calculation for a pumping speed of 2500 cu ft per second (as observed in some preliminary CO_2 experiments) gives an average residence time of 6 milliseconds and on the average fewer than two collisions with the walls before being condensed. For such results the calculation is not entirely valid, but shows clearly that the molecular velocity distribution is far from random. The ion gauge indication is therefore highly questionable. If any prediction is meaningful, the gauge is likely to read too high because of the molecules beaming from the inlet "diffuser", unless the gauge opening is shielded from this flux.

Under very high rates of pumping as indicated in the last example, the concept of pumping speed becomes questionable. To be meaningful, the pressure ahead of the pumping device should be measured sufficiently distant from the pump to be representative of the body of the gas, undisturbed by the loss to the pump. The

*Note: We are taking some liberty with terminology here. In the first place, an ion gauge is actually a density-measuring device although its results are customarily expressed as an equivalent pressure, with the gauge temperature implied. Secondly, the pressure in the chamber is strictly meaningful only for a gas completely confined in an isothermal box, where density and molecular velocity distribution are uniform over the volume. In engineering situations, this concept is frequently liberalized to include non-random conditions involving mass flow and non-uniform temperature, provided the variations from the mean over the volume are relatively small. In situations where the variations are not relatively small, the usual pressure concept is no longer valid and a more complex description of the physical situation must be employed.

higher the rate of pumping the wider region over which the distorting effect of the pump is significant, and the more sensitive the results are to the chamber geometry used. In this case, it seems more appropriate to treat the individual molecular processes rather than the gas as a continuous fluid, that is, to use a microscopic rather than a macroscopic description. This implies the use of an accommodation coefficient as a measure of the probability that a molecule incident on the cryo-array will not be scattered back into the chamber.

The distribution of temperature over the various bounding surfaces of the chamber must also be considered, because of its distorting effect on the flow pattern. During calibration only the shields were cooled, while during experimental runs additional surfaces were cooled, not always to the same temperature. Temperature effects are likely to be smaller than those due to the pumping effect. It is important to realize that any distortion of the flow pattern from being purely random can produce a difference between the corrected indications of two gauges (P1 and P6) at the reference plane, even though these gauges have been calibrated together statically.

3.4 Overall Accuracy of Pumping Speed Determinations

The accuracy to be expected of pumping speed determinations in this facility will depend on the extent to which the possible sources of error discussed above can be minimized. For individual measurements pumping nitrogen, it seems reasonable to expect that an uncertainty of $\pm$ 50% (95% confidence level) can be achieved. With a large number of measurements, the uncertainty in the best-fit pumping speed curve may very likely be less than $\pm$ 20%.

The effect of gas composition on pumping speed measurements must also be considered since the program has been concerned with the use of nitrogen, hydrogen, helium and carbon dioxide. Correction of ion gauge indications for gases other than nitrogen has been discussed in Section 2. The conductance of an orifice is dependent on gas composition, varying inversely as the square root of the molecular

weight. The conductance values chosen (whether calculated values, or values derived experimentally) should thus be multiplied by 3.73 when used for hydrogen, by 2.65 for helium, and 0.80 for carbon dioxide.

4. SUMMARY

Considerations in the use of hot-cathode ionization gauges for accurate pressure measurements have been reviewed, and operational procedures recommended. Modifications to gauge control circuits have been designed, and satisfactory operation of the units verified after the changes were made by ADL.

A McLeod gauge was provided as a standard, and the ion gauges calibrated against it. Correction curves were provided, and estimates made of the various sources of error. Using proper corrections, the overall uncertainty of individual static pressure measurements is estimated to be $\pm$ 40% (95% confidence level) assuming care and good technique are employed.

Correction factors for gases other than nitrogen have been provided.

An oil manometer was provided for mass flow rate calibration and ADL personnel familiarized with it. Errors in various methods of mass flow rate measurement have been discussed, particularly with respect to the metering orifice arrangement.

Errors in pumping speed determinations have been discussed, including both instrumental errors and the effects of non-random flow. The complications at very high pumping speeds are mentioned, since under these conditions the uncertainty in the results is considerably greater.

Estimates of the overall accuracy depend on many variables, but careful work is likely to give $\pm$ 50% (95% confidence level) for the uncertainty of individual pumping speed determinations. With a large number of measurements, the uncertainty in the best-fit pumping speed curve may very likely be within $\pm$ 20%.

REFERENCES

1. "Assessment of Experimental Determination of Pressure", NRC Memorandum No. 1, appended to ADL Progress Report for the period ending May 15, 1961.

2. "Assessment of Experimental Determination of Pumping Speed", NRC Memorandum No. 2, appended to ADL Progress Report for the period ending June 16, 1961.

3. Redhead, Paul A., "Errors in the Measurement of Pressure with Ionization Gauges", 1960 Vacuum Symposium Transactions. (Pergamon Press, London, 1961), p. 108.

4. Nottingham, Wayne B. and Franklin L. Torney, Jr., "A Detailed Examination of the Principles of Ion Gauge Calibration", 1960 Vacuum Symposium Transactions. (Pergamon Press, London, 1961), p. 117.

5. Clark, R. J., J. Sci. Instrum. 5, 126 (1928).

6. Wallis, W. A. and H. V. Roberts, Statictics, A New Approach (McGraw Hill, 1952), p. 449.

7. Jansen, C. G. J. and A. Venema, Vacuum, 9, 219 (1959).

8. Podgurski, H. H. and F. N. Davis, Vacuum, 10, 377 (1960).

9. Leck, J. H., "Pressure Measurement in Vacuum Systems", The Institute of Physics, London (1957), p. 69.

10. Dushman, Saul, Vacuum Techniques (John Wiley, New York,1949) p. 161-2.

11. Dushman, Saul, Vacuum Techniques (John Wiley, New York, 1949) p. 98-99.

12. Liepman, H. W., J. Fluid Mechanics, Feb. 1961, p. 65.

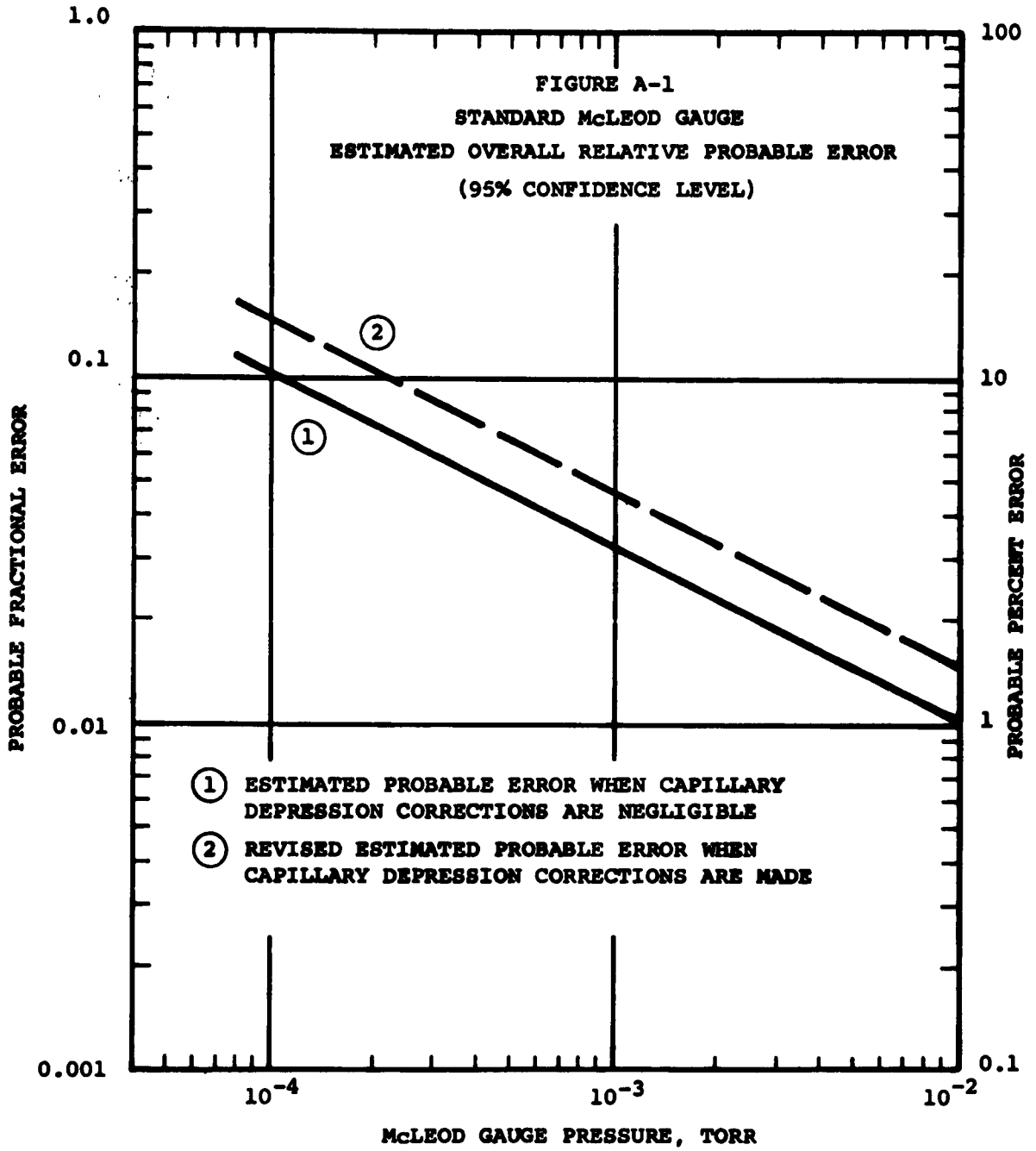
1.0
0.1
0.01
0.001
100
10
1
0.1
PROBABLE FRACTIONAL ERROR
PROBABLE PERCENT ERROR
10^{-4}
10^{-3}
10^{-2}
McLEOD GAUGE PRESSURE, TORR
FIGURE A-1
STANDARD McLEOD GAUGE
ESTIMATED OVERALL RELATIVE PROBABLE ERROR
(95% CONFIDENCE LEVEL)
1
2
1 ESTIMATED PROBABLE ERROR WHEN CAPILLARY DEPRESSION CORRECTIONS ARE NEGLIGIBLE
2 REVISED ESTIMATED PROBABLE ERROR WHEN CAPILLARY DEPRESSION CORRECTIONS ARE MADE

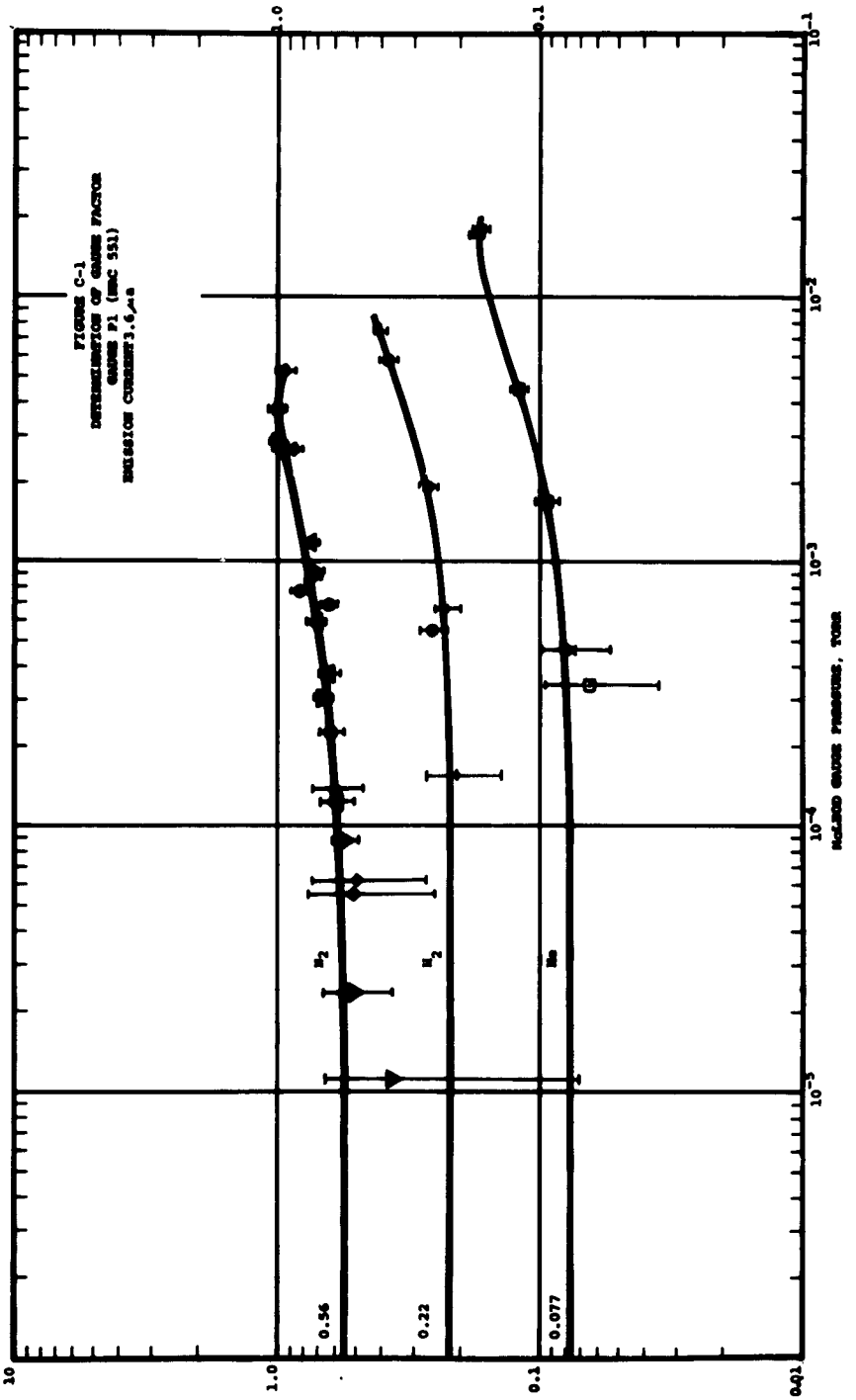
FIGURE C-1
DETERMINATION OF GAUGE FACTOR
GAUGE P1 (EMC 551)
EMISSION CURRENT=3.6 mA
10
1.0
0.1
0.01
1.0
0.1
10^{-1}
10^{-2}
10^{-3}
10^{-4}
10^{-5}
H_2
H_2
He
0.56
0.22
0.077
INDICATED GAUGE PRESSURE, TORR

ION GAUGE P_1 (NRC 551)

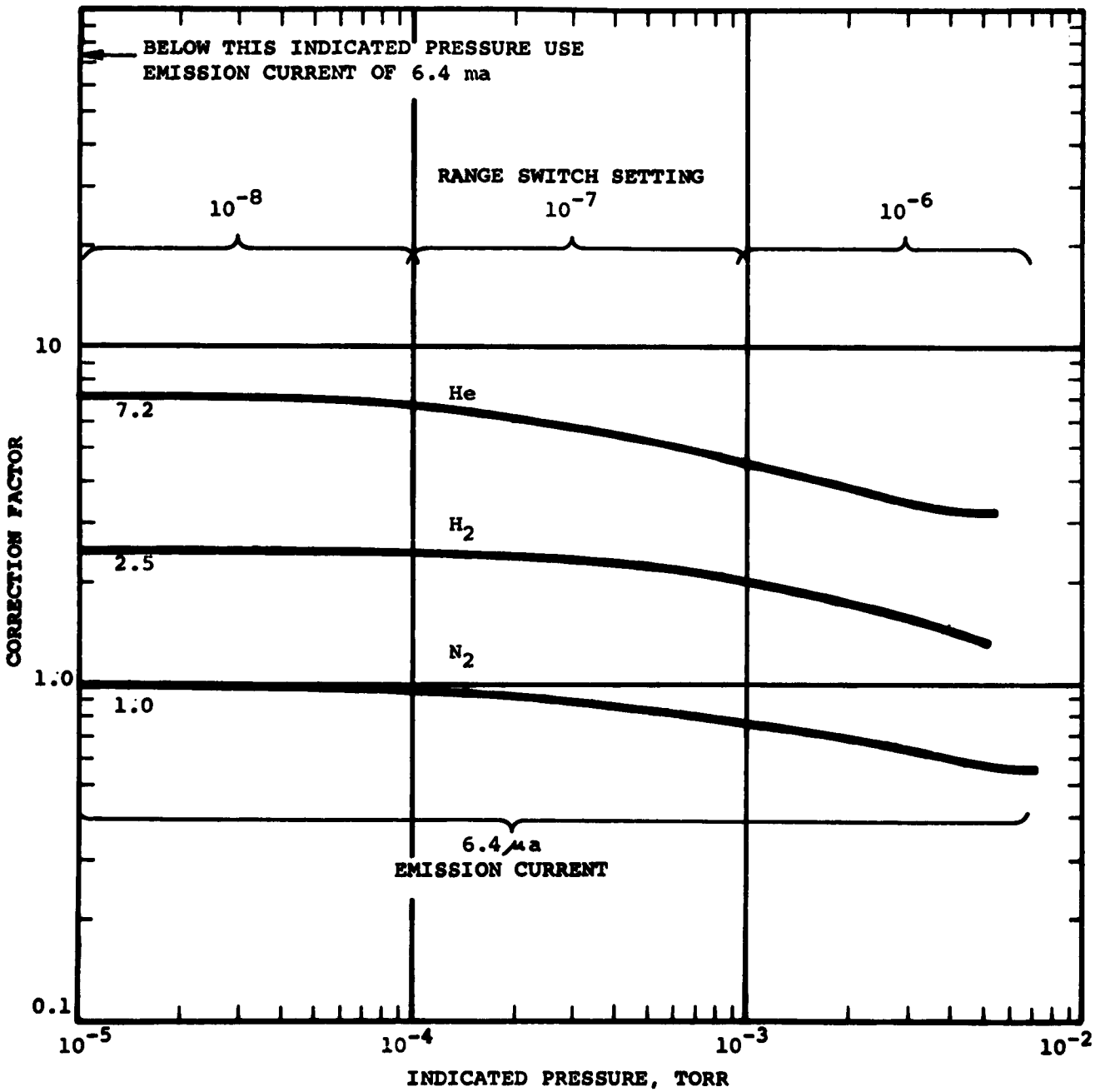

FIGURE D-2

Arnold Engineering Development Center
Arnold Air Force Station, Tennessee
Rpt. No. AEDC-TDR-62-57. RESEARCH STUDY OF CRYOPUMPING WITH A RADIATION SHIELDED CONDENSER. Final Technical Report, March 1962, 107 p. incl biblio., illus., tables. Unclassified Report

The purpose of this study was to develop information for the empirical design of a cryopumping array. Experiments with a chevron-shielded condenser have been carried out and, where possible, the results correlated with analysis. An array constructed from aluminum panels proved to be very serviceable. The array capture probability for nitrogen was about 0.2 and was essentially constant over the range of pressures from 10^{-8} to 5×10^{-6} torr; above 5×10^{-6} torr the capture probability increased with pressure. CO_2 was cryopumped on the chevron shields. Hence, the capture probability has high, varying from 0.7 to 0.94 in the pressure range from 5×10^{-7} to 7×10^{-5} torr. The greatest transmission of radiation through the chevrons to the condenser occurred with a CO_2 deposit on the chevrons and a nitrogen deposit on the condenser, and with infrared radiation incident on the inlet to the array. Even under these conditions less than 2 percent of the incident irradiation was transmitted to the condenser. As a result of our study, we conclude that cryopumping by means of a condenser at 20 K, radiation shielded by surfaces cooled to 77 to 100 K, can provide effective means for removal of nitrogen and all less volatile gases from a vacuum space in the ultra-high vacuum range.

1. Cryogenics
2. Refrigerant condensers
3. Shielding
4. Vacuum systems
5. Nitrogen
6. Instrumentation
7. Measurement
8. Design
9. Pumps
10. Diffusion
11. Aluminum
I. AFSC Program Area 850E, Project 7778, Task 777801
II. Contract AF 40(600)-899
III. Arthur D. Little, Inc., Cambridge, Mass
IV. Raymond W. Moore, Jr.
V. Available from OTS
VI. In ASTIA Collection

Arnold Engineering Development Center
Arnold Air Force Station, Tennessee
Rpt. No. AEDC-TDR-62-57. RESEARCH STUDY OF CRYOPUMPING WITH A RADIATION SHIELDED CONDENSER. Final Technical Report, March 1962, 107 p. incl biblio., illus., tables. Unclassified Report

The purpose of this study was to develop information for the empirical design of a cryopumping array. Experiments with a chevron-shielded condenser have been carried out and, where possible, the results correlated with analysis. An array constructed from aluminum panels proved to be very serviceable. The array capture probability for nitrogen was about 0.2 and was essentially constant over the range of pressures from 10^{-8} to 5×10^{-6} torr; above 5×10^{-6} torr the capture probability increased with pressure. CO_2 was cryopumped on the chevron shields. Hence, the capture probability has high, varying from 0.7 to 0.94 in the pressure range from 5×10^{-7} to 7×10^{-5} torr. The greatest transmission of radiation through the chevrons to the condenser occurred with a CO_2 deposit on the chevrons and a nitrogen deposit on the condenser, and with infrared radiation incident on the inlet to the array. Even under these conditions less than 2 percent of the incident irradiation was transmitted to the condenser. As a result of our study, we conclude that cryopumping by means of a condenser at 20 K, radiation shielded by surfaces cooled to 77 to 100 K, can provide effective means for removal of nitrogen and all less volatile gases from a vacuum space in the ultra-high vacuum range.

1. Cryogenics
2. Refrigerant condensers
3. Shielding
4. Vacuum systems
5. Nitrogen
6. Instrumentation
7. Measurement
8. Design
9. Pumps
10. Diffusion
11. Aluminum
I. AFSC Program Area 850E, Project 7778, Task 777801
II. Contract AF 40(600)-899
III. Arthur D. Little, Inc., Cambridge, Mass
IV. Raymond W. Moore, Jr.
V. Available from OTS
VI. In ASTIA Collection